Universitetet I Trondheim
Norges Tekniske Høgskole
Institutt for Eksperimentalfysikk

Wave Power Project
Mechanical Engineering Department
University of Edinburgh

Magnetic Squeeze-Films

Design Proposals for a magnetic-repulsion enhanced hydrostatic bearing for the type N2 wave-power buoy

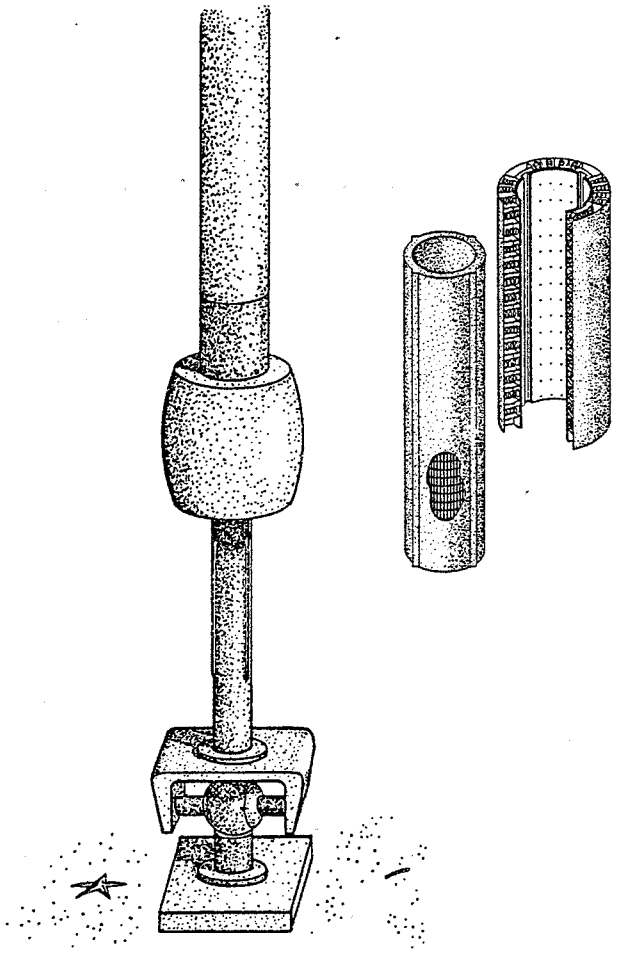

April, 1983

DESIGN PROPOSALS FOR A MAGNETIC-REPULSION ENHANCED HYDROSTATIC BEARING FOR THE TYPE N2 WAVE-POWER BUOY.

A report commissioned and funded by the Norwegian Institute of Technology (Division of Experimental Physics), at the University of Trondheim, Norway.

Colin G. Anderson

April 1983

Department of Mechanical Engineering
University of Edinburgh
Mayfield Road
Edinburgh EH9 3JL

CONTENTS

LIST OF FIGURES

LIST OF TABLES

SYMBOLS

A	Magnetic repulsion quadratic coefficient (Pa)
a_2	Magnet length
B	Magnetic repulsion quadratic coefficient (Pam^{-1})
b	Bearing axial length
b_1 , b_2	Magnet cross-sectional dimensions
C	Magnetic repulsion quadratic coefficient (Pam^{-2})
C_D	Drag coefficient
c_1 , c_2	Magnet cross-sectional dimensions
d	Magnet-sheet depth
e	Relative displacement of buoy and mooring pipe
e_s	" " under max. static load
e_c	" " under max. cyclic load
F_D	Drag force
$F_v(z)$	Vertical magnetic repulsion force per unit volume
F_y	Horizontal magnetic repulsion force
F_z	Vertical magnetic repulsion force

Table 1 *List of the more important symbols and abbreviations used in the report; S.I. units are used in all calculations. For practical reasons, some dimensions are expressed in millimetres, and some loads in tonnes force.*

SYMBOLS

g	Gravitational acceleration ($9.815 ms^{-2}$)
H	Gross bearing clearance
H_o	" " " in equilibrium condition
H_s	" " " under max. static load
H_c	" " " under max. cyclic load
H_{ci}	Intrinsic coercivity of magnetic material (Am^{-1})
h	Water film thickness (ie narrow bearing clearance)
h_o	" " " in equilibrium condition
h_s	" " " under max. static load
h_c	" " " under max. cyclic load
J	Magnetisation (tesla)
K	Mechanical springs' pressure constant (Pam^{-1})
k	Mechanical spring constant, single spring (Nm^{-1})
ℓ	Compression spring length
ℓ_e	" " " in unloaded (free) condition
ℓ_s	" " " fully compressed (solid height)
N_s	No. of compression springs per unit area

Table 1 (contd.)

SYMBOLS

P_m	Magnetic repulsion pressure
P_s	Compression spring pressure
P_w	Water pressure
q	Fluid volume flow rate (squeeze film calculations)
R	Bearing outer radius
R_e	Reynolds number
r	Bearing inner radius
t	Plastic sheet thickness (covering magnet system)
W	External load
W_s	Static load
y	Magnets' lateral offset
z	" pole separation
$\alpha, \alpha_c, \beta, \gamma$	Abbreviations used in analysis (see pp 31-2)
θ	Angle with resultant load line-of-action
ϕ	Non-linear damping coefficient
μ	Fluid viscosity (water = 10^{-3} $Nm^{-2}s$, air = $1.8 \times 10^{-5} Nm^{-2}s$)
μ_o	Magnetic constant ($4\pi \times 10^{-7} Hm^{-1}$)

Table 1 (contd.)

1. DESIGN REQUIREMENTS

1.1 Low Friction

This requirement is fundamental to any bearing; values of friction coefficient f for some common systems are:

	f
plain bearing - teflon	0.12 - 0.04
commercial ball bearings	10^{-1} - 10^{-3}
hydrodynamically lubricated surfaces	10^{-2} - 10^{-3}
hydrostatically lubricated surfaces	10^{-3} - 10^{-6}

(after Rabinowicz (ref. 1))

In the case of a power buoy experiencing an average total horizontal load of 18 tonnes force and moving with a peak heave velocity of 4.0 ms^{-1} (ref. 2) the power lost due to friction is given by

$$P = 4{\cdot}0 \times 18\,000 \times g \times f \quad \text{watts} \qquad (1)$$

Taking f = 0.1, the power loss is 71kW, or ca 18% of the peak rated output of 400kW (ref. 3); with f = 0.001 these values reduce to o.71kW and 0.18% respectively.

1.2 Standing Forces

The buoy system will experience non-reversing loads due to local tidal currents and wind resistance; a 'worst-ever' case might involve a current of 2ms^{-1} and windspeed of 70ms^{-1} . We shall consider first the forces on the buoy itself.

The drag force exerted on a sphere by a fluid of density ρ kgm^{-3} and velocity **u** ms^{-1} is given by

$$F_D = 0.5 \times \rho \times A \times u^2 \times C_D \quad \text{newtons} \qquad (2)$$

in which the projected frontal area $\mathbf{A} = \pi r^2$ metres^2 and the dimensionless drag coefficient $\mathbf{C_D}$ depends on the Reynolds number **Re** of the system, given by

$$Re = \frac{\rho l u}{\mu} \qquad (3)$$

where l is taken as the sphere diameter = $2 \times r$

For a sphere in air with **r** = 5m, and $\mu = 1.8 \times 10^{-5} Nm^{-2}s$, $\rho = 1.3\ kg\ m^{-3}$, and taking **u** = $70ms^{-1}$ the Reynolds number is approximately 5 x 10^7. For the same sphere in water, for which $\mu = 10^{-3}\ Nm^{-2}s$, $\rho = 10^3\ kgm^{-3}$, and using **u** = $2ms^{-1}$, **Re** = 2 x 10^7. At such high values of **Re**, $\mathbf{C_D}$ tends towards a constant value of 0.2 (ref.4) as shown in Fig 1(a).

As the buoy will almost certainly be heaving unlatched in the kind of conditions suggested above we will assume it to be half submerged, and take the total drag force to be the wind resistance of the upper half plus the water resistance of the lower. Dealing firstly with the upper half, from equation (2)

$$F_D\ (\text{upper}) = \frac{0.5 \times \rho_{air} \times \pi \times 5^2 \times 70^2 \times 0.2}{2}$$

$$= 25.0\ kN \qquad (4)$$

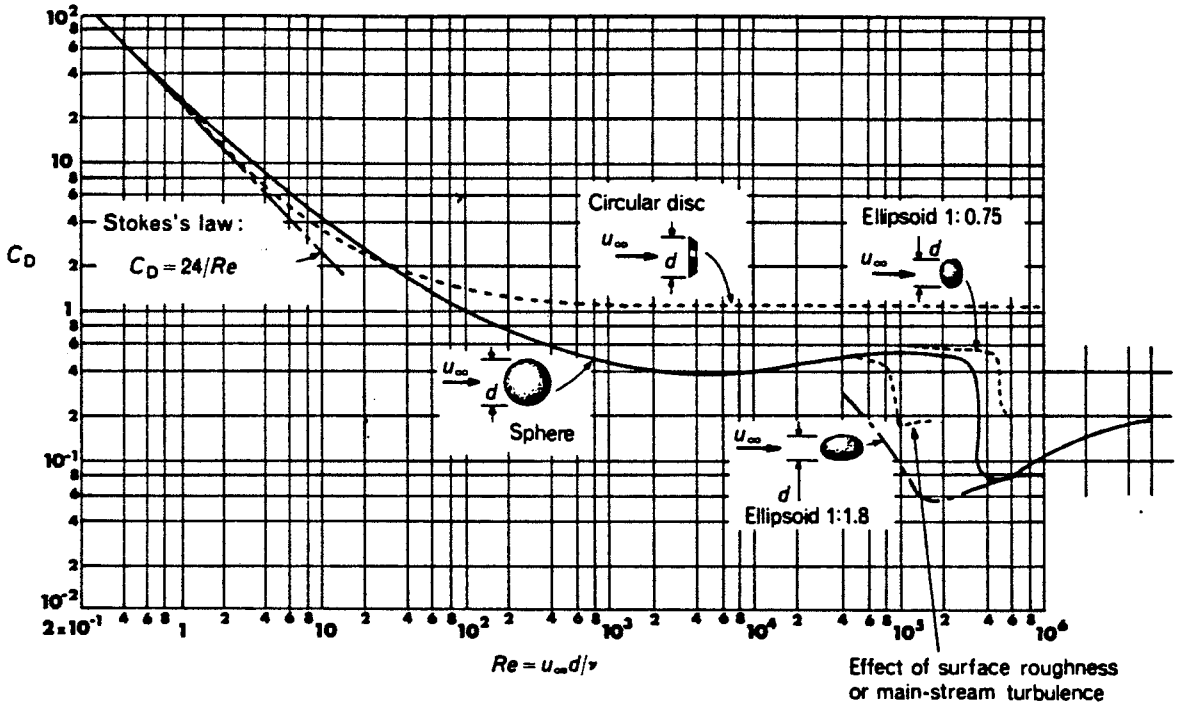

FIG. 1a Drag coefficients of smooth, axially-symmetric bodies

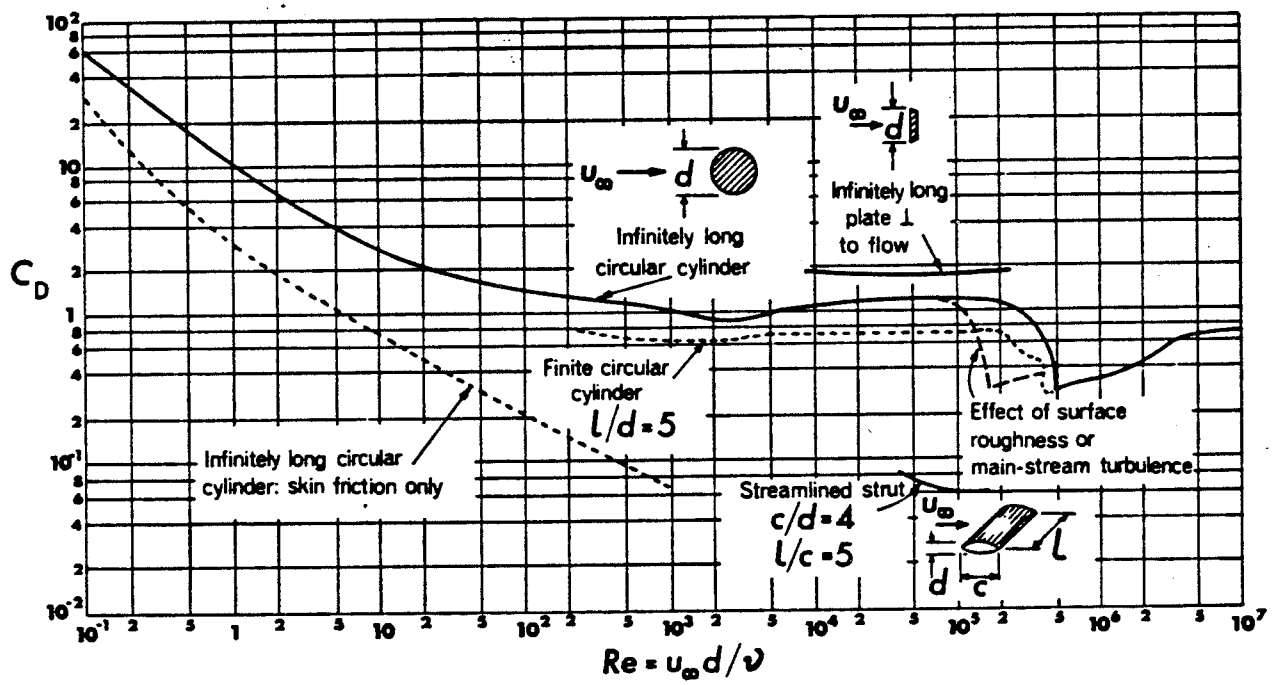

FIG. 1b Drag coefficient for two-dimensional bodies

Fig 1 Drag coefficients vs Reynolds number for (a) spheres, and (b) cylinders (reprinted from ref 4).

For the lower half of the buoy:

$$F_D\ (lower) = \frac{0.5 \times \rho_{water} \times \pi \times 5^2 \times 2^2 \times 0.2}{2}$$

$$= 15.7\ kN \qquad (5)$$

thus giving a total drag force of 40.7kN (4.15 tonnes f).

To allow for the possibility of the buoy being less than half submerged, we should perhaps take the maximum standing force to be $2 \times \mathbf{F_D}$ (upper) = 50kN (5.1 tonnes force)

The part of the bearing associated with the buoy counter-weight will always be submerged, and so we consider only its water resistance. Assuming a cylindrical counterweight of diameter **d** = 4m (say), in water with **u** = $2ms^{-1}$ then from equation (3) with ℓ = **d** the Reynolds number is given as 8×10^6. From fig 1(b) the corresponding drag coefficient $\mathbf{C_D}$ is seen to be ca 0.8. For reasons explained later in this report, the projected area of the part of the bearing under water may be around $40m^2$; using equation (2) with **A** = $40m^2$, **u** = $2ms^{-1}$ and $\mathbf{C_D}$ = 0.8, the drag force is 64kN (6.52 tonnes f).

1.3 Cyclic Loading

The major loads the bearing must sustain will be those forces acting normal to the mooring pipe and originating in the cyclic action of the waves. Their precise causes have been detailed (ref.2) and a summary of the values expected can be seen in Fig 2. Assuming the most extreme wave, the upper assembly (A + B) would experience 300kN (30.6 tonnes f) and the lower (C + D) 500kN (50.9 tonnes f).

It will be assumed that the horizontal loads have the same magnitude in both directions during each cycle; in Fig 3 the results are shown of surge-force tests carried out on a horizontal-axis cylinder in regular waves of various frequencies (ref.5). In each case the peak surge forces

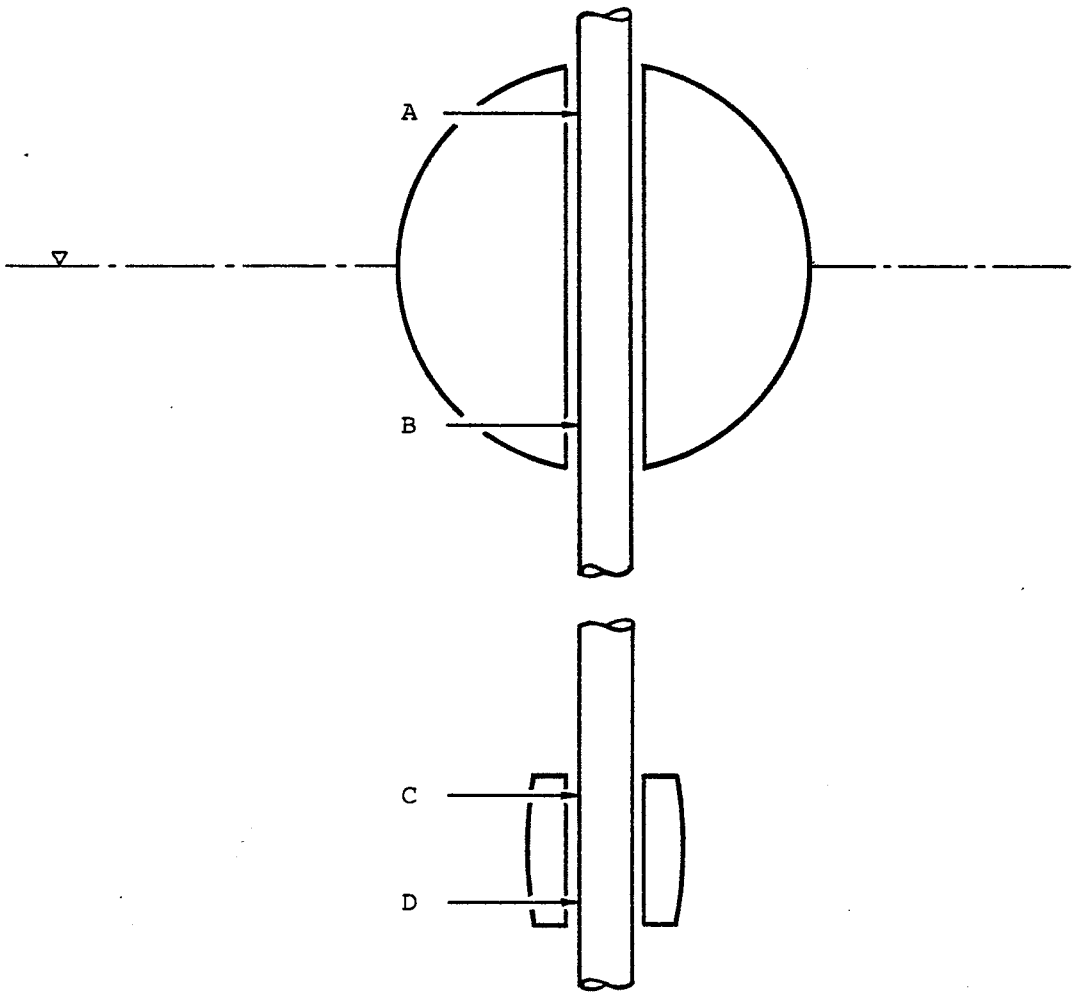

A: mean load 50kN, maximum load 150kN
B: " " " " " "
} A+B: max load 300kN

C: mean load 40kN, maximum load 250kN
D: " " " " " "
} C+D: max load 500kN

Fig 2 Cyclic wave loads, experimentally predicted (ref 2).

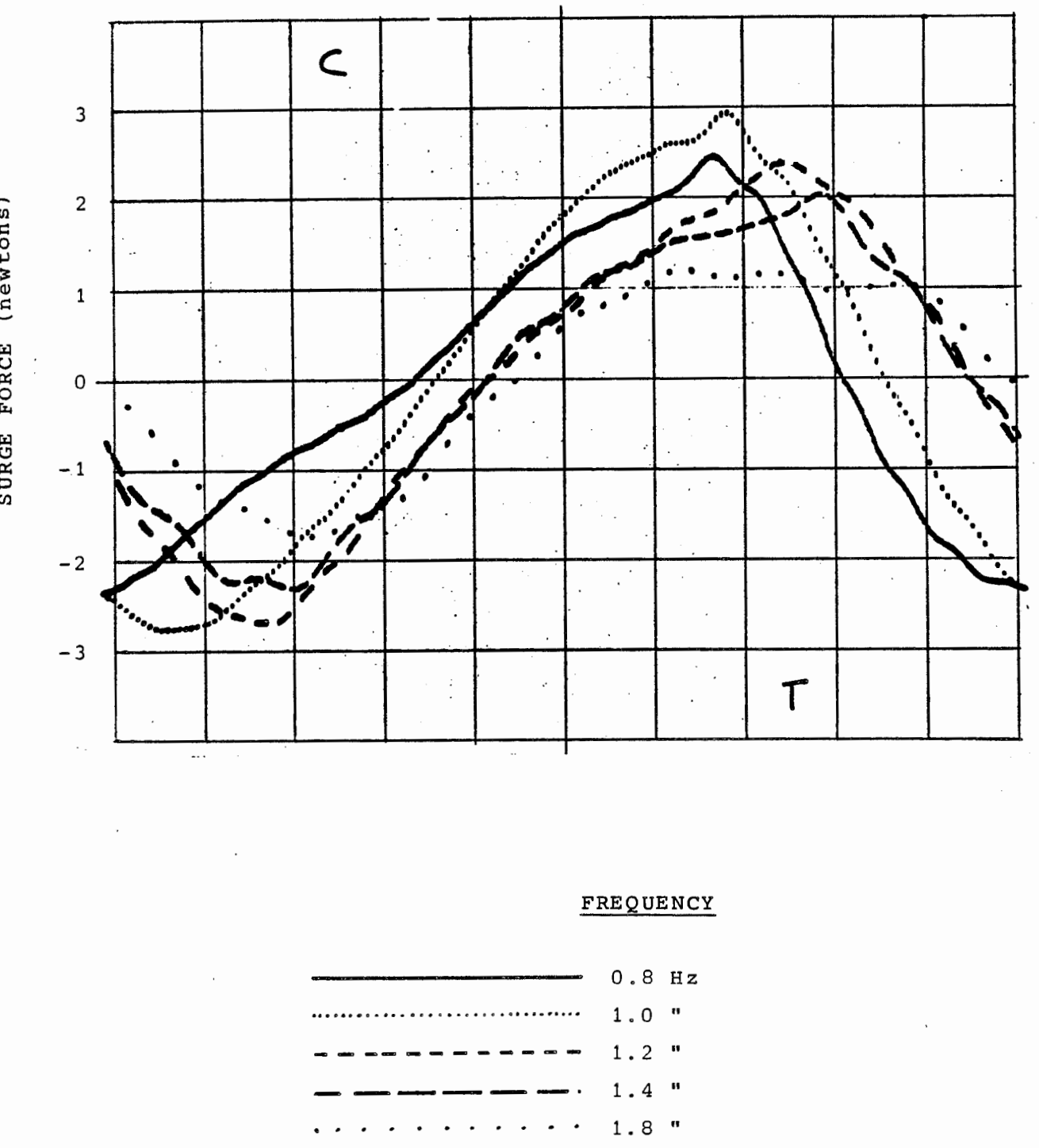

Fig 3 Surge forces on a horizontal-axis cylinder at various wave frequencies. Model diameter = 10cm, waterline depth = 5cm, (reprinted from ref 5).

in both directions are very nearly the same, and this will be assumed to apply to spheres as well as cylinders. The average wave period is 10 seconds, the time taken for full load reversal simply half this figure, i.e. 5 seconds.

1.4 Construction Details

The bearing design must be made compatible with the latching mechanism of the buoy (required for most economic operation) but without occupying any significant proportion of the buoy's internal diameter. It should also be easy to build and to instal.

1.5 Tolerances

The greatest deviations in mooring pipe geometry are incurred during its construction, with the circularity of a 1.4m diameter pipe of wall thickness 25mm being guaranteed to $\pm$ 2.5mm. The flexure of such a pipe under normal operating loads will be small by comparison, shown by considering an extreme case: if we assume the bending moment **M** at a section of the pipe to be so great that the maximum tensile stress σ_x equals the yield strength of the material, then the corresponding radius of curvature **R** can be found from elementary beam theory, according to

$$R = \frac{E y}{\sigma_x} \qquad (6)$$

where **E** is the modulus of elasticity and **y** the distance of the point from the neutral axis - in this case **y** is the pipe radius. For a typical steel **E** might be $2 \times 10^{11}\ Nm^{-2}$ and the yield strength $3 \times 10^{8}\ Nm^{-2}$; taking **y** = 0.7m the resultant radius of curvature from (6) is 467m, equivalent to a deflection of 1.1mm per metre length at the yield limit of the pipe. The corresponding value of **M** is found from

$$M = \frac{E I}{R} \qquad (7)$$

for which $I = \frac{\pi}{64} \left(d^{4}_{outer} - d^{4}_{inner} \right)$, in this case 0.0255, giving a fairly unlikely bending moment of 10.9 MNm.

1.6 Environmental Factors

All submerged offshore structures are subject, to a greater or lesser extent, to the problems of marine fouling, and corrosion or other chemical degradation. The effects of these must not be allowed to impair the operation of the bearing or to shorten its lifespan.

1.7 Lifespan

The target is fully submerged, maintenance-free operation for 20 years (ref. 2).

1.8 Cost

The cost of the bearing must be minimised within the constraints implied by 1.1 - 1.7 above.

2. OPERATING PRINCIPLES OF THE PROPOSED BEARING

2.1 Why a Hydrostatic Bearing?

A magnetic-repulsion enhanced hydrostatic bearing is proposed for the following reasons:

(i) The presence of a lubricating medium - water - is guaranteed; it would seem a shame not to use it.

(ii) Although both hydrodynamic and hydrostatic bearings afford very low friction coefficients (see section 1.1), the former would be ineffective if the buoy was latched, or at low heave velocities.

(iii) A hydrostatic design offers us the opportunity of distributing the loads evenly over the entire bearing surface, in direct contrast to a roller-guided system, which concentrates the loads.

(iv) In a true hydrostatic bearing the load is supported *entirely* by the viscous lubricating medium, without solid contact occuring between the bearing surfaces. Consequently, wear of these is reduced almost to zero.

(v) Although hydrostatic bearings are often associated with high-precision applications, such as turbine journal bearings, they may equally be used in applications involving non-uniform surfaces (ref. 6) or even non-rigid surfaces (ref. 7).

2.2 Magnetic Repulsion Enhancement

The definition of a hydrostatic bearing is one in which the lubricating fluid is externally pressurised and fed to the bearing surfaces; some form of pump is required for this purpose. The possibility of installing a powered pumping system on the buoy is ruled out on the grounds of cost and reliability. Because the big wave loads are cyclical, however, wave action can itself be used as the pumping system: the principle may be explained by referring to figure 4.

NOT TO SCALE

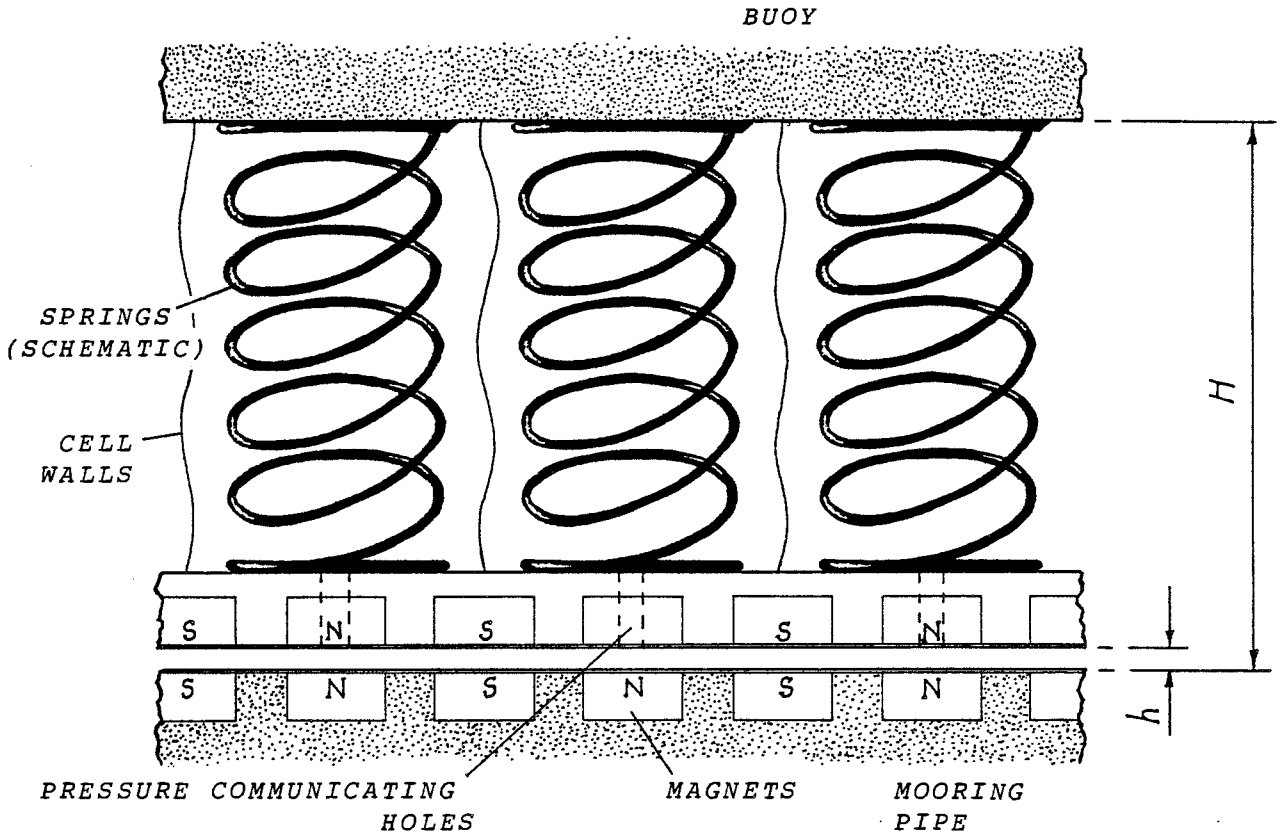

Fig 4 Schematic illustration of magnetic-repulsion enhanced hydrostatic bearing. Note that this simple spring arrangement will not be used in the actual power-buoy bearing, and is shown here only to convey the general principle.

The two rigid bearing surfaces are separated by a water-filled clearance of depth **H**. Attached to one of the surfaces is an array of compression springs, which are in turn attached to a semi-stiff sheet; firmly fixed to this are permanent magnets with their magnetic axes oriented in opposition to similar magnets, attached directly to the opposing bearing surface. The gap between the upper rigid surface and the magnet-sheet is divided into cells by flexible, but impermeable, fabric walls. Small holes are situated at intervals in the sheet, each representing a pressure-communicating hole in the base of one compression cell.

The important features of this arrangement are:

(i) The water in a cell may only flow in or out via the pressure-communicating hole in the sheet, but can do this quite freely. As a consequence, the water pressure in a cell is the same as that in the narrow clearance *just outside the hole*.

(ii) In the narrow clearance **h**, water may flow in any direction and will be governed only by the *horizontal* water pressure gradient, dP_w/dx.

(iii) The magnets, which are in mutual *repulsion* have a (nonlinear) spring rate which, for the range of vertical movement allowed, is much greater than that of the mechanical springs; the values of the two rates are chosen such that the narrow clearance **h** tends to zero as the gross separation **H** approaches its minimum allowable value.

(iv) The mechanical springs are precompressed to ensure that the initial value of **h** is small.

These characteristics give the bearing the following properties:

(a) The narrow clearance **h** is a function only of the gross separation **H**, and is independent of the water pressure **Pw**.

(b) The total pressure the bearing can withstand will be the sum of the water pressure and the spring pressure; because the springs and magnets are in series, the magnet pressure equals the spring pressure.

(c) From Stefan's law for squeeze films, the load supported by a viscous liquid flowing unidirectionally through a narrow slot is inversely proportional to the clearance *cubed* (ref 6): as the only flow of water tangential to the bearing is that in the narrow clearance (see fig 4) then the effective squeeze-film thickness is **h**, only a small fraction of the gross clearance **H**. Furthermore, the load is directly proportional to the rate of approach of the two rigid surfaces, ie dH/dt rather than the rate at which the squeeze-film thickness decreases (dh/dt), as is the common case.

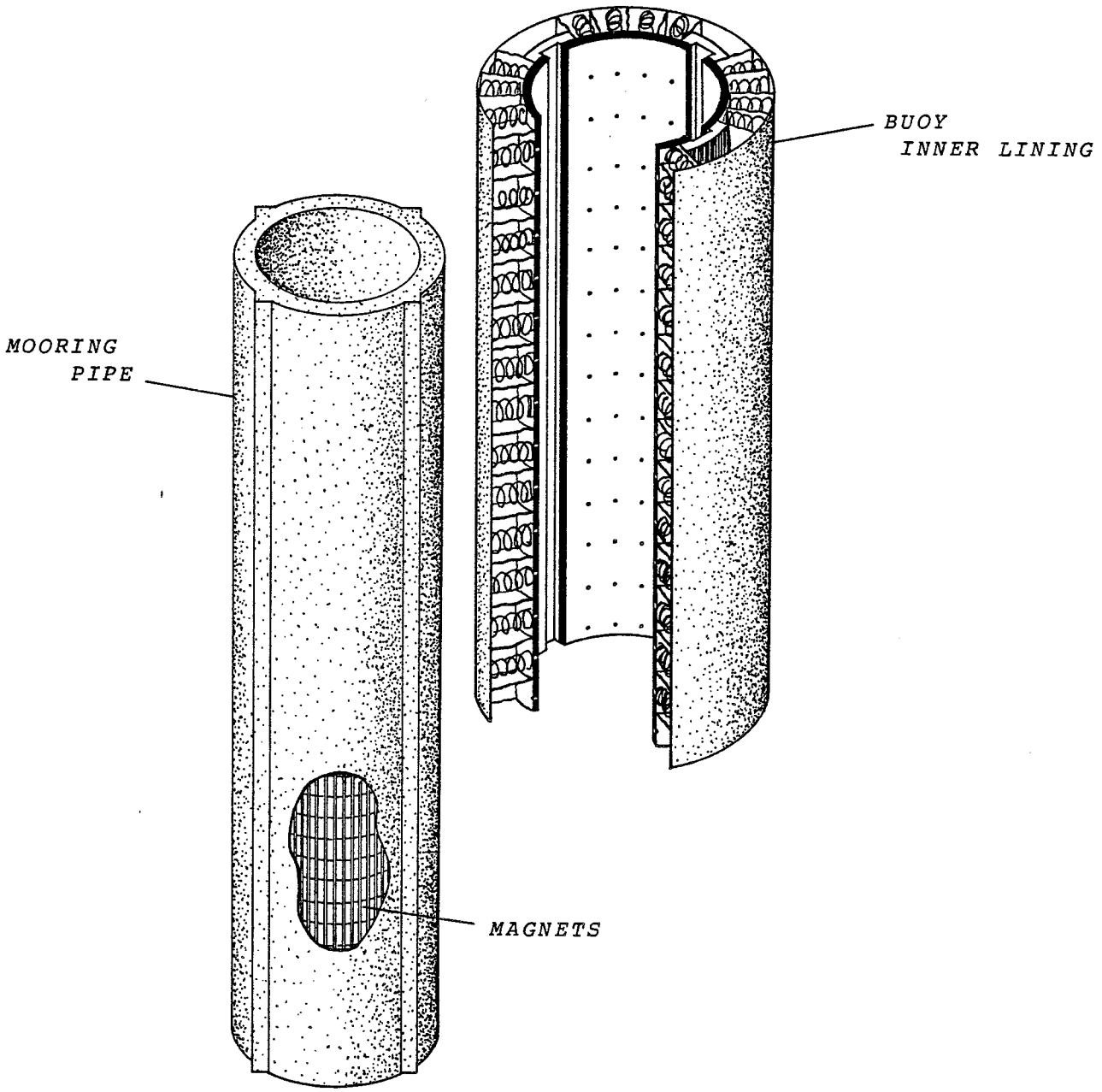

Fig 5 *The proposed power-buoy bearing (schematic). The four splines welded to the mooring pipe form part of the yaw-prevention system, other details of which have been omitted for clarity.*

Figure 5 is a schematic illustration of the power-buoy bearing. The collapsible cell layer desribed above forms an annular lining to the buoy, with permanent magnets arranged in axial rows along the length of its inner surface. Opposing magnets are laid along the mooring pipe in rows of the same circumferential pitch as those on the buoy; in bòth cases a protective plastic sheet covers the magnet surfaces. The four splines welded along the pipe belong to the yaw-prevention system discussed in section 5: further details of this have been omitted from fig 5 for clarity.

It is important to note that although figures 4, 5 and 6 depict the cells with conventional helical coil springs, there are good reasons why the springs actually used will not be as simple as this (see section 5): the illustrations are intended to clearly convey the *principle* of the bearing's operation, although the calculations of optimum spring constant etc. will be much the same in any case.

2.3 The Bearing in Operation

The operating characteristics of the enhanced hydrostatic bearing are illustrated in figs 6(a)-(c).

Figure 6(a) shows the unloaded, equilibrium situation. The large and small bearing clearances have initial values of H_o and h_o respectively, and these values are the same at all points around the bearing circumference.

Fig 6(b) shows the bearing under the maximum *static* load. The relative displacement of buoy and pipe, given the symbol **e** (for eccentricity) has reached its maximum static value e_s. This is the greatest load to which magnetic repulsion alone will be subjected, and the magnet system is optimised accordingly. The relative velocity de/dt is zero, and hence the water pressure **Pw** in the bearing is everywhere zero (ie ambient).

Note (i) the variation in **h** from its minimum value h_s at $\theta = 0$ (point of load application) to a maximum value at $\theta = \pi$: while the cells on one side of the bearing have reduced in volume to some extent, those on the other side have enlarged correspondingly.

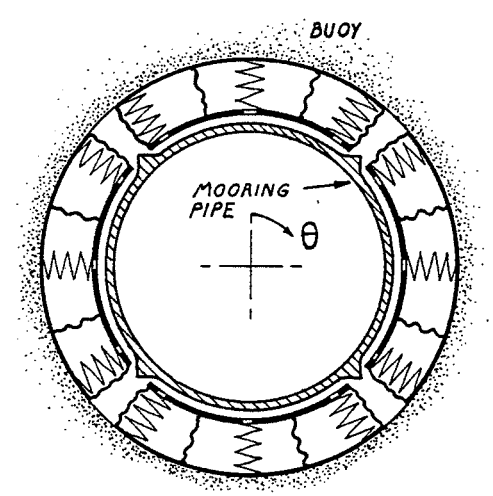

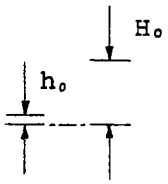

6(a) *Unloaded condition*

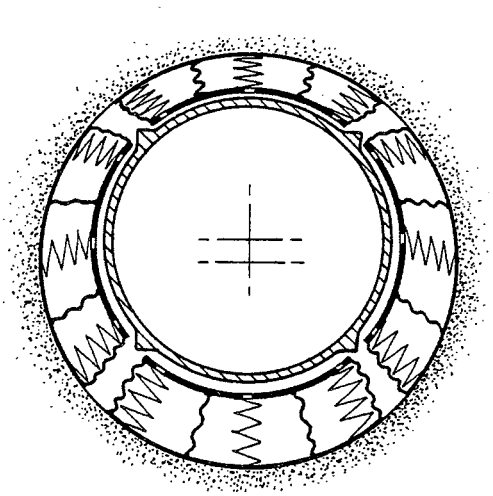

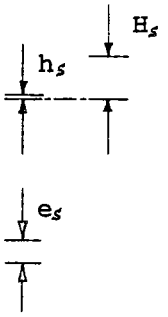

6(b) *Maximum static load*

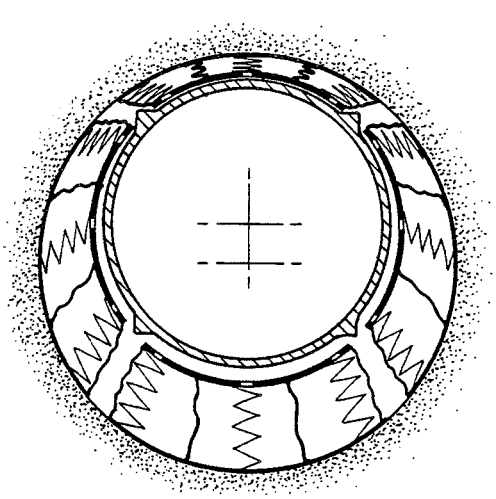

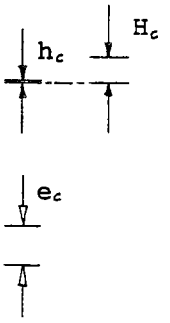

6(c) *Maximum cyclic load*

Fig 6 Operating characteristics of the bearing. Proportions are not to scale, and springs/cells are schematic only.

(ii) a relative radial displacement of **e** at $\theta = 0$ causes a similar *tangential* displacement at $\theta = \frac{\pi}{2}$; in order to prevent misalignment of opposing magnets a yaw-prevention system must be included. Although this is shown only schematically in fig 6 the effect of tangential shear on the springs at angles around $\theta = \frac{\pi}{2}$ is clear, highlighting the unsuitability of a simple helical coil spring system.

In fig 6(c) the maximum cyclic load is in effect; the large water pressure forces which have built up in the narrow clearance - now at its minimum value $\mathbf{h}_c$ - prevent the bearing surfaces from making contact, even though the applied load is many times the maximum magnetic repulsion force. While the cells on one side of the bearing collapse, those diametrically opposite open up, effectively recharging with water. The process is greatly aided by increased values of **h** in this region. (ie around $\theta = \pi$), and springs and magnets must be chosen with this maximum value of **h** in mind.

The principle of operation is very similar to that observed in the joints of large animals, where two layers of cartilage pressed together slowly exude synovial fluid into a narrow clearance, in a process known as "weeping" lubrication (refs 8 & 9). The layers themselves are compressed only according to their stiffness, while the major load (which can be as much as 1 ton f in^{-2} (ca 15 MNm^{-2})) is supported by fluid pressure; the apparently "ill-fitting" nature of the joints is in fact to allow the compressed cartilage to recharge with fluid when unloaded.

The power-buoy collapsible cell lining is analogous to a single layer of cartilage, in our case the fluid recharge being effected by the cyclic action of the waves. Although the bearing application is novel, then, the principle is anything but: "weeping" bearings have been in continuous production and use for several hundred million years.

2.4 Design Considerations

For the proposed bearing to work as described above, the following features must be incorporated into the design:

(i) The cell compression-spring rate must be unaffected by relatively large excursions in shear. As described above, the maximum shear deformation of the springs occurs at ca 90° to the maximum compressive deformation, but the actual displacements in the two cases are very nearly equal.

(ii) The flexible cells must be able to collapse and to shear, but must not contract or expand other than by allowing water to flow through the pressure communication holes. If the cells were highly elastic, there would be the tendency for a net flow of water round the bearing *outside* the narrow clearance.

(iii) A yaw prevention mechanism must be accommodated which completely restricts the magnet sheets from moving circumferentially, allows them to move through small radial excursions corresponding to the expected variation in clearance **h**, and offers no resistance to the axial (heave) motion of the bearing.

(iv) The magnet sheet must be designed to have a certain degree of compliance in order to prevent small deviations in pipe diameter from affecting the squeeze-film thickness, which must be determined only by the local spring and magnet forces. However, the magnets themselves must be allowed only two degrees of freedom, namely restricted radial translation and free axial translation.

(v) the latching brake system may have to be accommodated within the length of the bearing.

The solutions to these problems are discussed later in this report, following an analysis of the performance of the proposed design.

3. ANALYSIS

3.1 Introduction

In this section an attempt is made to estimate the static and cyclic loads that could be supported by a repulsion-enhanced hydrostatic bearing; a general analysis of this kind is essential before the design of specific components can be finalised. At various points throughout the procedure, it will become necessary to introduce certain assumptions and simplifying approximations, and in each case the reasons for doing so will be fully explained.

Fig 7 shows the geometry of the bearing to be considered in this analysis.

3.2 Static Load Calculation

As no hydrostatic pressure can be developed when the relative movement of buoy and mooring pipe, ie $^{de}/_{dt}$, is zero the maximum static load **Ws** must be supported entirely by magnetic repulsion (see section 2.3).

On the application of a constant load **Ws** the buoy will be displaced relative to the pipe a distance e_s (see figs 6(b) and 7): the resulting combination of increased magnetic repulsion on the loaded side of the bearing, where the magnets' clearance **z** decreases, and reduced repulsion on the 'leeward' side where **z** increases, acts to balance the load. Note that the contributions from both sides are equally important.

We shall begin by examining a small section of the magnetic sheet, at an angle θ to the point of load application (see fig 8), in equilibrium under the forces acting on it, namely:

(i) magnetic repulsion, radial (F_1) and tangential (F_2).

(ii) compression spring forces, radial (F_3) and tangential (F_4).

(iii) sheet internal forces; in shear, tension/compression, and bending

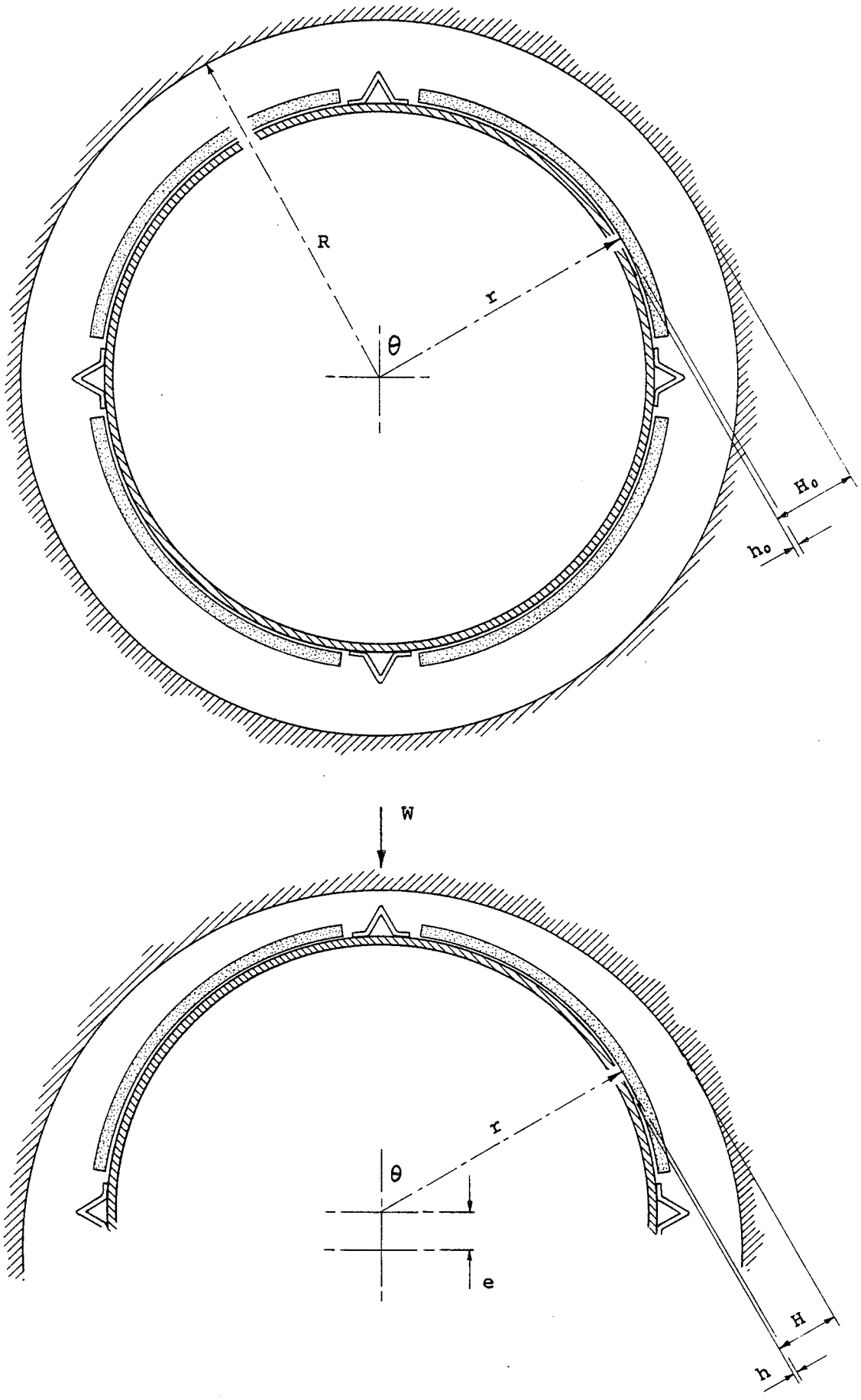

Fig 7 Bearing geometry (ca 1/15 scale). The springs have been omitted for clarity; see table 1 for full explanation of terms.

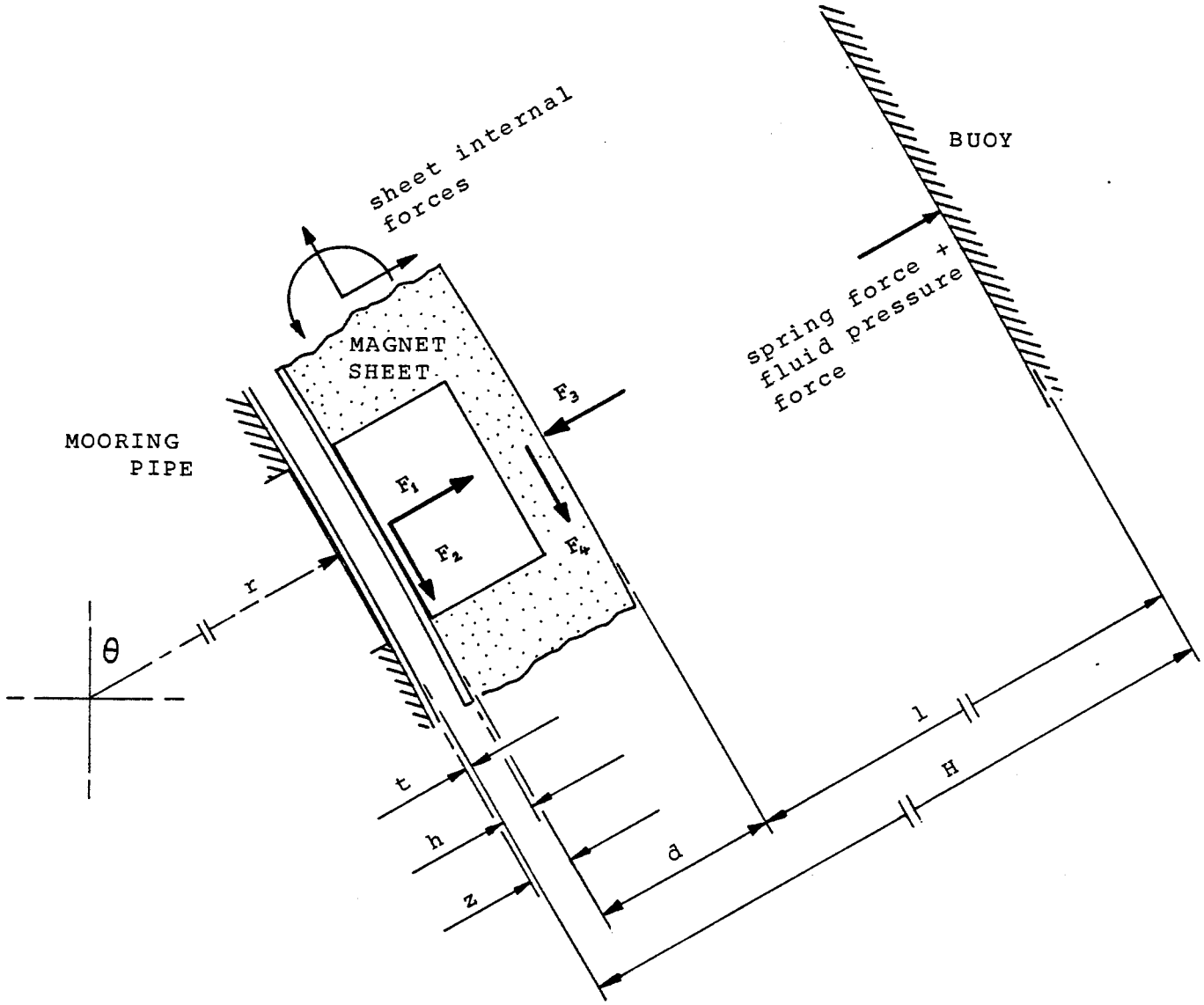

Fig 8 *Forces on a small section of the bearing at an angle θ to the point of load application. For static load calculations we consider only those forces which act on the magnet-sheet.*

Because of the rotation (yaw) prevention system - described later - the tangential magnetic force F_2 will be very small, and may be disregarded for the moment. We will return to it later in a discussion of the yaw prevention mechanism. The tangential spring force F_4 will be low by design: we have almost complete freedom in this respect and can, if we wish, choose a rate an order of magnitude lower than the (already low) spring compression rate.

A combination of this last force (F_4) and a different balance of radial magnetic and spring forces F_1 and F_3 on adjacent sections of the sheet will give rise to the other forces depicted in fig 8, the sheet internal forces. The yaw alignment system is present to ensure that the tangential components of these counteract the forces F_2 and F_4. The two essential requirements for the magnet sheet are that the magnets themselves should maintain a constant cirumferential spacing with no tendency to pitch or roll, and that the local radial forces F_1 and F_3 be the only ones to determine the clearance **h**.

The sheet, then, will have to be rigid on a local scale, ie one or two magnet widths, but relatively flexible on a larger scale, say one tenth of the bearing circumference. We can show, however, that the deviations in sheet radius involved will be very small, and that the right choice of sheet material and cross-section can easily satisfy the 'semi-rigid' criterion, allowing us to make the approximation that the magnet clearance **z**, and film thickness **h** depend only on F_1 and F_3. Thus we shall disregard the internal stresses in the sheet when calculating its load-supporting characteristics; they must however be re-introduced in future consideration of its actual design.

From figure 8, then, the incremental sheet section is in equilibrium under forces F_1 and F_3; the magnet's face separation is **z**, the water film thickness is **h**. The spring force F_3 may be expressed as pressure **Ps** times area; area is given as **brdθ** where **r** is the bearing radius and **b**, assuming the load to apply evenly along the whole *length* of the bearing, is its axial length. Spring force on the section is then given by

$$F_3 = P_s \, b \, r \, d\theta \quad \text{newtons} \tag{8}$$

Similarly magnet force is found from pressure **Pm** according to

$$F_1 = P_m \, b \, r \, d\theta \quad \text{newtons} \tag{9}$$

Equating (8) and (9) gives the obvious condition for equilibrium, ie that the two pressures are equal:

$$P_m = P_s \tag{10}$$

If the unloaded length of a compression spring is ℓ_e metres and its compressed length under some arbitrary load is ℓ m, then the restoring force it exerts is given by Hooke's law as $\mathbf{k}(\ell_e - \ell)$ newtons, where **k** is the spring rate in newtons per metre deflection. Assuming **Ns** springs, evenly distributed, per square metre of bearing surface area, we can replace the force constant **k** with a spring pressure constant **K**, where

$$K = N_s k \quad \text{Pa per metre deflection} \tag{11}$$

The official SI unit of pressure, the pascal (Pa), is here used instead of Nm^{-2} in order that the units of **K** help convey its physical significance.

The spring pressure on the bearing element is then given as

$$P_s = K (\ell_e - \ell) \quad \text{pascals} \tag{12}$$

where the local spring length ℓ is a function of buoy displacement **e** and **θ**.

From the geometry of figure 7, **H** varies with **e** and **θ** according to

$$H = \sqrt{R^2 - e^2 \sin^2\theta} - r - e\cos\theta \qquad (13)$$

and the equilibrium value H_o (when **e** = 0) is given as

$$H_o = R - r \qquad (14)$$

For small values of H_o and **e**, as encountered in journal bearing calculations (refs 1 (Archibald) and 6), expression (13) is often approximated to

$$H = H_o - e\cos\theta \qquad (15)$$

For our purposes this approximation is not as good, becoming worse at large values of **e**, and values of **θ** around 60–120°. However, for static load calculations the error in **H** should not exceed 3–4% of the true value: furthermore, in cyclic load calculations the fluid film which supports almost the whole load acts predominantly over a narrow angle centred around the load application point (**θ** = 0), where the error in **H** is small. We shall use the approximate formula for **H**, then, and in table 2 are listed typical values of the errors to be expected by doing so.

From fig 8 the local spring length ℓ is given as

$$\ell = H - d - z \quad \text{metres} \qquad (16)$$

and, substituting for **H** from (15)

$$\ell = H_o - e\cos\theta - d - z \quad \text{metres} \qquad (17)$$

the local spring pressure is then found from (12)

$$p_s = K(\ell_e + e\cos\theta + d + z - H_o) \quad \text{pascals} \qquad (18)$$

θ (degrees)	e=0mm	50	100	150
0	zero	zero	zero	zero
30	"	+0.21	+1.17	+4.42
60	"	+0.57	+2.71	+7.69
75	"	+0.66	+2.91	+7.41
90	"	+0.66	+2.71	+6.34
105	"	+0.58	+2.23	+4.88
120	"	+0.44	+1.61	+3.35
150	"	+0.14	+0.46	+0.91
180	"	zero	zero	zero

Table 2 *% error in gross bearing clearance H incurred by using the approximate expression (15) rather than the exact one (13); based on an outer radius R of 950mm, inner radius r = 750mm, hence* H_o *= 200mm.*

The magnet pressure **Pm** is a non-linear function of pole separation **z**; we shall, at a later stage, attempt to find a suitable empirical function **Pm(z)** to closely approximate the pressure characteristics over the range of clearances envisaged. Provisionally, a range of **z** of 0 - 20mm will be used.

In the meantime, we continue by calculating the maximum static load which the bearing can sustain for a given displacement e_s, in terms of the mechanical spring characteristics only.

If we treat the moving part of the bearing, ie that attached to the buoy, plus the buoy itself, as a single body in equilibrium under external forces, then from fig 7 these forces are seen to consist only of the applied load **Ws** and magnetic repulsion pressure forces. From equation (8) the magnitude of the repulsion force acting on a small section of the bearing at an angle **θ** to the applied load was given as **Pmbrdθ** newtons. The only component of this force which actually opposes the load is that which acts parallel to it, ie: **Pmbrcosθdθ**. The total load **Ws** then equals the integral of the incremental repulsion forces round the circumference of the bearing, ie

$$W_s = \int_0^{2\pi} P_m \, b \, r \cos\theta \, d\theta \qquad \text{newtons} \tag{19}$$

From equation (10) we may substitute **Ps** for **Pm**, and furthermore replace **Ps** according to (18) with $K\left(l_e + e_s\cos\theta + d + z - H_o\right)$

giving

$$W_s = Kbr\int_0^{2\pi}\left(l_e + e_s\cos\theta + d + z - H_o\right)\cos\theta \, d\theta \tag{20}$$

which may be re-written as

$$W_s = Kbr\left(l_e + d - H_o\right)\int_0^{2\pi}\cos\theta \, d\theta + Kbr\int_0^{2\pi}\left(z\cos\theta + e_s\cos^2\theta\right)d\theta \tag{21}$$

where the first integral is simply zero, leaving

$$W_s = Kbr \int_0^{2\pi} (z \cos\theta + e_s \cos^2\theta)\, d\theta \qquad (22)$$

By making a small approximation, it is possible to obtain a relatively useful result: from fig 8 it is seen that **z** is always quite small compared with the spring length ℓ and so from (17) we make the approximation that

$$\ell = H_o - e_s \cos\theta - d \quad \text{metres} \qquad (23)$$

and hence, by analogy with (18), spring pressure is given by

$$P_s = K(\ell_e + e_s \cos\theta + d - H_o) \quad \text{pascals} \qquad (24)$$

and by analogy with (19) - (22), total static load is found from

$$W_s = Kbr \int_0^{2\pi} e_s \cos^2\theta\, d\theta \quad \text{newtons} \qquad (25)$$

which can be integrated to give the approximate solution

$$W_s = Kbr\pi e_s \quad \text{newtons} \qquad (26)$$

In other words, by neglecting the small difference the magnets' clearance **z** makes to the springs' deflection we find that the bearing behaves as a simple linear spring, with deflection e_s directly proportional to applied load **Ws**, the 'spring constant' being given as **Kbr**π. This result will be extremely valuable in future calculations of the dynamic behaviour of the bearing under cyclic loads, when we can make the approximation that the contribution to the total bearing resistance supplied by magnetic repulsion is proportional to the displacement **e**, thus corresponding to the 'spring' component of a dynamic system. In general, then:

$$W_{magnetic} \simeq Kbr\pi e \quad \text{newtons} \qquad (27)$$

3.3 Hydrostatic load calculation

An accurate estimate of the loads which the bearing can sustain with hydrostatic pressure is not really feasible at the present time. Until experiments are carried out to determine the squeeze-film characteristics of a cell system with compound spring behaviour, of the type proposed, any calculations of hydrostatic load must be considered as tentative only.

Although an attempt is made here to find an analytical solution, some fairly crude approximations are made, especially regarding fluid-flow characteristics; the laws of scaling for fluid-mechanical problems are well known, but the need for an appropriate experimental model remains imperative if flow behaviour is to be predicted. Except in a few fairly simple cases, purely analytical predictions will be of strictly limited worth, and the following calculation should be regarded in that light.

We will try to calculate the load which may be supported by water pressure alone, when the relative velocity de/dt is non-zero. We shall disregard the magnetic repulsion component of total force for the moment, but reintroduce it when we examine the combined load characteristics of the bearing.

From the theory of squeeze-films (ref 1 (Archibald)), the volume flow rate **q** of a viscous liquid between parallel plates is given by

$$q = \frac{\Delta P_w \, b \, h^3}{12 \mu \ell} \qquad (28)$$

where the pressure drop Δ **Pw** and flow are both in the direction of the slot length ℓ with the slot width **b** being assumed much greater than ℓ; **h** is the film thickness (see fig 9). With reference to fig 8 we take the bearing axial length to correspond to the slot-width **b** and make the assumption that, because **b** is much greater than the diameter **D**, the preferred direction of flow will be circumferential. This approximation, when applied to journal bearings, is good when **b** is more than about four times the diameter **D** (ref 6). For the power-buoy bearing the ratio **b/D** is likely to be greater than this, but the two cases are by no means

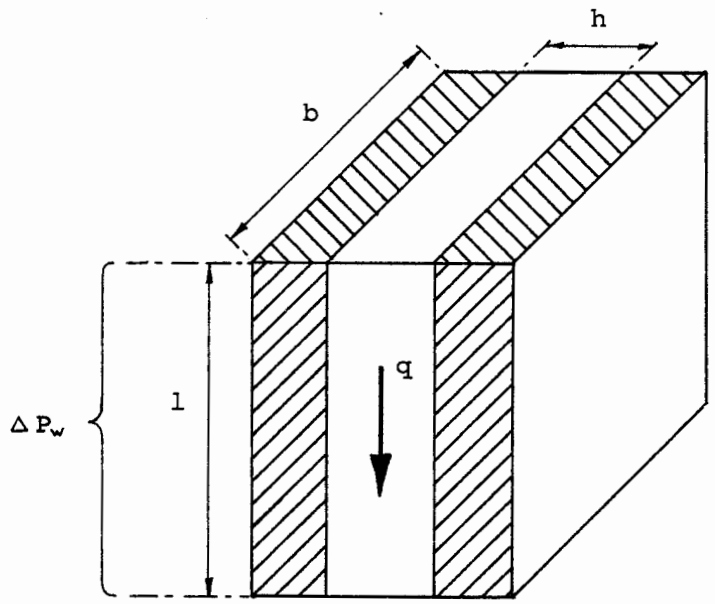

Fig 9 Dimensions for squeeze-film calculations.

strictly comparable. In all real cylindrical hydrostatic bearings some degree of axial flow will take place, and the amount of this remains an element of uncertainty in our calculation.

From fig 8 again, we replace ℓ in (28) with the circumferential length **rdθ** of the bearing element, the circumferential pressure drop over this length being given as **dPw**. Equation (28) may then be re-written

$$q = -\frac{bh^3}{12\mu r} \times \frac{dP_w}{d\theta} \qquad (29)$$

(The negative sign allows us to specify **q** a positive quantity, as $dP_w/d\theta$ will always be negative.)

The flow rate **q** will depend on the local value of **h**, the relative radial velocity of buoy and pipe de/dt, to some extent the axial heave velocity, and the nature of the flow itself.

In this context we introduce the following approximations:

(i) flow rate in the clearance **h** will be governed by viscous shear forces, with fluid inertia being neglected.

(ii) flow will be assumed laminar only.

(iii) flow rate will be a function of the hydrostatic pressure gradient $dP_w/d\theta$ only, with the effects of relative buoy/pipe heave motion disregarded; **h** will be assumed independent of axial position, with zero pressure gradient in the axial direction.

Approximations (i) - (iii) introduce the second area of uncertainty into the calculation. At large values of clearance **h**, there will be little viscous resistance, and the squeeze-film flowrate **q** will be dominated by fluid inertia (ref 10). As a consequence, a calculation which ignores

fluid inertia will be valid only in those regions of the bearing where **h** is sufficiently narrow. However, to determine the value of **h** where viscous flow becomes the dominant factor will require a rigorous mathematical treatment, plus the design and testing of a suitable experimental model; in the meantime we continue to assume viscous-only flow, aware that this may seriously underestimate the load capacity of the bearing.

Because there are two directions of relative motion - radial and axial - the flow itself *if laminar* will consist of two components: the first of these, due to the pressure gradient $\frac{dP_w}{d\theta}$ set up by the radial movement, is Poiseuille flow, and occurs with a parabolic velocity profile across the clearance **h**. The second, Couette flow, is caused by the shearing action of relative axial movements and gives rise to a linear velocity distribution across the clearance.

To complicate matters, the flow may not be laminar at all. The Reynolds number applicable to the system may be higher that the critical value above which flow becomes turbulent. Prediction of the flow characteristics is not easy, as the film represents a cross between a boundary layer and a squeeze-film, each of which has a different definition of Reynolds number. We must remember too that steady flow patterns take a finite time to establish, and our fluid film is acting for only 5 seconds or so. Adding to all this the uncertain effect of the cell-outlet geometry on the flow pattern, we resort to approximations (i) - (iii) above.

Supposing wholly *turbulent* flow, the likely effects would be, by increasing viscous friction, to increase both the buoy drag and the squeeze-film delay time. An earlier estimate of viscous drag power-loss based on laminar flow (ref 11) gave a value of ca 1.4kW; even if turbulent film conditions led to a factor of ten increase in this figure it would still represent less than 4% of the peak rated output of 400kW. Any increase in film delay time can be counted as a positive advantage.

Returning to the calculation of hydrostatic pressure, then, we may derive another expression for the volume flow rate **q**: from the symmetry

of fig 7(b) the instantaneous rate of displacement of water past a radial section of width **H** and angle **θ** is simply the projected area of the mooring pipe from the symmetry axis to **θ** multiplied by the rate of approach de/dt hence

$$q = b r \sin\theta \times \frac{de}{dt} \tag{30}$$

because of the operating characteristics of the compressible cell layer, as described in sections 2.2 - 2.4, the net circumferential flow of water given by (30) must all take place in the narrow clearance **h**, where the flow-rate was determined by (29). Equating these two, then

$$\frac{-b h^3}{12 \mu r} \times \frac{dP_w}{d\theta} = b r \sin\theta \times \frac{de}{dt} \tag{31}$$

and hence

$$\frac{dP_w}{d\theta} = \frac{-12 \mu r^2 \sin\theta}{h^3} \times \frac{de}{dt} \tag{32}$$

From fig 8 the film thickness **h** is equal to **z - 2t**, where **t** is the thickness of the plastic covering the magnets' surface; we may further substitute for **z** according to the following procedure:we first approximate the magnet pressure **Pm** by a quadratic of the form

$$P_{m(z)} = A + Bz + Cz^2 \tag{33}$$

in which **A**, **B** and **C** are experimentally determined coefficients. Then, equating **Pm** and **Ps** as in equation (10), and then from (18),

$$A + Bz + Cz^2 = K(l_e + d + z + e\cos\theta - H_o) \tag{34}$$

rearranging (34) gives

$$Cz^2 + (B-K)z + A - K(l_e + e\cos\theta + d - H_o) = 0 \tag{35}$$

which has solutions

$$z = \frac{K - B \pm \sqrt{(K-B)^2 - 4C\left[A - K(l_e + e\cos\theta + d - H_o)\right]}}{2C} \qquad (36)$$

and by investigation the correct solution is found to be the smaller (i.e. *subtracting* the square-root term). We express **z** more neatly by

$$z = \alpha + \beta(\gamma + e\cos\theta)^{\frac{1}{2}} \quad \text{metres} \qquad (37)$$

where

$$\alpha = \frac{K - B}{2C} \quad \text{metres}$$

$$\beta = -\sqrt{\frac{K}{C}} \quad \text{metres}^{\frac{1}{2}}$$

$$\gamma = \frac{(K - B)^2}{4CK} + l_e + d - \frac{A}{K} - H_o \quad \text{metres}$$

Equation (37) then gives us the magnet pole-separation **z** as a function of angle **θ** and buoy displacement **e**, in terms of magnetic and mechanical spring constants, and constant physical dimensions.

Substituting, then, for **h** in (32)

$$\frac{dP_w}{d\theta} = \frac{-12\mu r^2 \sin\theta}{(\alpha - 2t + \beta[\gamma + e\cos\theta]^{\frac{1}{2}})^3} \times \frac{de}{dt} \qquad (38)$$

and introducing the notation $\alpha_c = \alpha - 2t$, from which

$$\frac{dP_w}{d\theta} = \frac{-12\mu r^2 \sin\theta}{(\alpha_c + \beta[\gamma + e\cos\theta]^{\frac{1}{2}})^3} \times \frac{de}{dt} \qquad (39)$$

To find the relationship of water pressure **Pw** to angle **θ** we integrate (39) giving

$$P_w(\theta) = \frac{-12\mu r^2}{\beta^2 e} \times \frac{de}{dt} \times \left\{ \frac{\alpha_c + 2\beta[\gamma + e\cos\theta]^{\frac{1}{2}}}{(\alpha_c + \beta[\gamma + e\cos\theta]^{\frac{1}{2}})^2} + Ci \right\} \qquad (40)$$

Evaluation of the constant of integration **Ci** leads us into another area of difficulty. If the bearing were ideal, with no film leakage axially or at the spline positions (see fig 7) the boundary condition would be **Pw** = 0 at **θ** = π. These assumptions (particularly the latter) seem optimistic, but allocating a smaller value to the "zero-Pw" angle is unhelpful as it implies negative film pressures at **θ** greater than this angle. We will keep the zero-Pw angle general for the moment, denoting it **θ₀**, the full expression for **Pw** then being given as

$$P_w(\theta) = \frac{12\mu r^2}{\beta^2 e} \times \frac{de}{dt} \times \left\{ \frac{\alpha_c + 2\beta[\gamma + e\cos\theta_0]^{\frac{1}{2}}}{(\alpha_c + \beta[\gamma + e\cos\theta_0]^{\frac{1}{2}})^2} - \frac{\alpha_c + 2\beta[\gamma + e\cos\theta]^{\frac{1}{2}}}{(\alpha_c + \beta[\gamma + e\cos\theta]^{\frac{1}{2}})^2} \right\} \qquad (41)$$

The total load **Ww** supported by water pressure alone is found by integrating **Pw** over the entire bearing area, using the same procedure as for the magnet pressure case (see equation (19)), and hence

$$W_w = \int_0^{2\pi} P_w \, b r \cos\theta \, d\theta \qquad (42)$$

Integration of this expression has not yet been achieved analytically, but numerical solutions may be fairly easily found. If we divide the surface of the bearing into **n** parallel axial strips of equal area, the circumferential length of each will be $\frac{2\pi r}{n}$ and hence its area = $\frac{2\pi rb}{n}$. The angle of the **i**th strip from the load-axis will be $\frac{2\pi i}{n}$ and if the fluid pressure it experiences is **Pw(i)** then the component of force acting to oppose the load will be given by **Ww(i)**, where

$$W_w(i) = \frac{2\pi rb}{n} \times P_w(i) \cos\left(\frac{2\pi i}{n}\right) \qquad (43)$$

The total load supported by hydrostatic pressure is then found from

$$W_w = \frac{2\pi rb}{n} \sum_{i=1}^{n} P_w(i) \cos\left(\frac{2\pi i}{n}\right) \qquad (44)$$

We now consider the ideal case where the position of zero (ambient) fluid pressure is diametrically opposite that of maximum pressure, ie $\theta = \pi$ in equation (41). Now, hydrostatic pressure **Pw** is directly proportional to velocity, and when de/dt equals zero so too does **Pw** everywhere in the bearing. If the direction of motion reverses, ie de/dt becomes negative, it seems reasonable to assume that the zero-pressure angle θ is now *zero*, and the maximum value of **Pw** at $\theta = \pi$. Using equation (44) with this assumption the following result is noted: with the bearing displaced a given distance **e** from equilibrium, the hydrostatic resistance to moving it at **v**ms^{-1} from this position is exactly the same as the resistance to moving it at **-v**ms^{-1} *from the same position*. In other words, it is apparently as hard to squeeze the fluid film out as it is to squeeze it in. The reasons for this are as follows:

(i) equation (41) was derived on the basis of viscous flow only, and took no account of fluid inertia.

(ii) the pressure gradient $dP_w/d\theta$ varies only with displacement **e**, angle θ and clearance **h** (se equation (32)). We know, however, that **h** is itself a function of **e** and θ and so by keeping these constant and reversing the velocity de/dt the sign of $dP_w/d\theta$ changes, but its magnitude does not.

This phenomenon is predicted by Stefan's law for the case of two infinitely wide rectangular surfaces separated by a viscous fluid (ref 6): the load required to force the surfaces together at a given rate is the same as that required to pull them apart at the same rate (with the load inversely proportional to the clearance cubed), provided there is no pressure gradient at right angles to the direction of flow, and that fluid inertia is neglected.

The situation described above is illustrated in figures 10(a) and (b). Fig 10(a) shows the variation of (left) $dP_w/d\theta$, (centre) **Pw**, and (right) **Pw**cosθ with angle θ for a given combination of de/dt and **e**. In fig 10(b) the displacement **e** is unchanged, but the velocity de/dt is reversed and as a result the sign, but not the magnitude, of $dP_w/d\theta$ (left) is changed for all angles θ; the pressure distribution **Pw** (centre) changes accordingly, but the total supported load, given by the *net* area under the curve of **Pw**cosθ (right) is the same in both cases, although of course, in different directions.

The situation which has been considered is very much idealised; in reality the combination of a high fluid pressure gradient and large bearing clearance **h** will probably result in flow rates being dominated by inertial, rather than viscous, forces. Indeed, at any given moment, all three types of flow - viscous laminar, viscous turbulent and inertial - will be present in different regions of the bearing, but an analysis made on this basis would require a great deal more time than can be devoted to it in this report.

A calculation of this sort may seem to be of most use only in highlighting the areas where the greatest uncertainty exists, and further

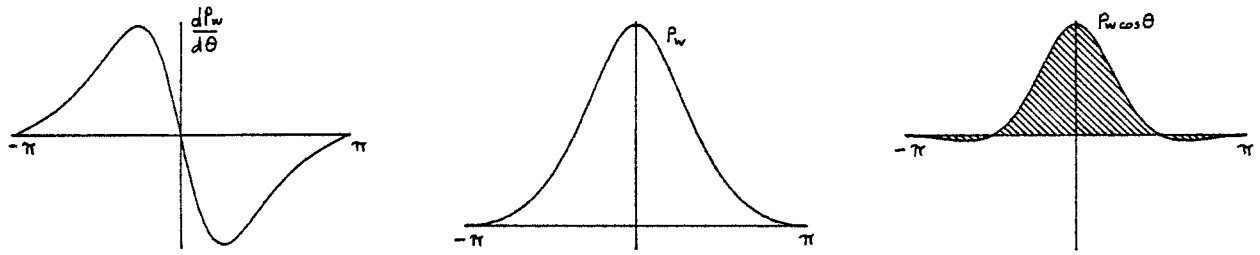

(a)

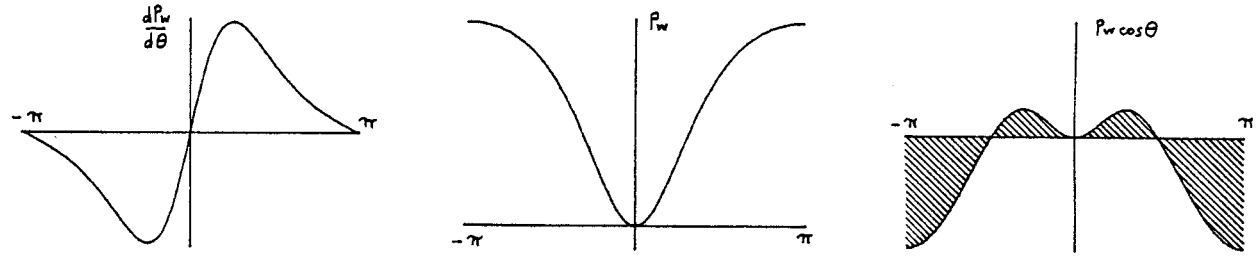

(b)

Fig 10 *Hydrostatic pressure characteristics of an idealised enhanced squeeze-film bearing, illustrating the effect of load reversal:*

(a) Variation in (left) $dP_w/d\theta$, (centre) P_w, and (right) $P_w \cos\theta$ with angle θ from the point of maximum load.

(b) As (a), but with reversed velocity (de/dt now negative); displacement e is unchanged.

reinforcing the call for experimental measurements. However, although the numbers predicted by such a treatment may prove to be of little value, the form of the result is of some interest: from equations (41) and (42), the expression for the bearing resistance due to hydrostatic pressure may be written as the product of the relative velocity $\frac{de}{dt}$ and a complicated function of **e** and an integral in **θ**. If we call this function ϕ then

$$W_w = \phi \frac{de}{dt} \tag{45}$$

where

$$\phi = \frac{12\mu b r^3}{\beta^2 e} \int_0^{2\pi} \left\{ \frac{\alpha_c + 2\beta\left[\gamma + e\cos\theta_o\right]^{\frac{1}{2}}}{\left(\alpha_c + \beta\left[\gamma + e\cos\theta_o\right]^{\frac{1}{2}}\right)^3} - \frac{\alpha + 2\beta\left[\gamma + e\cos\theta\right]^{\frac{1}{2}}}{\left(\alpha + \beta\left[\gamma + e\cos\theta\right]^{\frac{1}{2}}\right)^3} \right\} \cos\theta \, d\theta \tag{46}$$

In terms of a dynamic system, ϕ corresponds to a nonlinear damping coefficient; a thorough treatment of this problem might be based on the analytical or experimental determination of the precise nature of ϕ.

3.4 Combined load characteristics

A "first-pass" prediction of the combined load behaviour of the bearing under dynamic loading conditions might be made on the following basis:

(i) the driving force is the *net* force acting on the outside of the power buoy in a direction perpendicular to the mooring pipe, including surge force, drag, buoyancy components, etc.

(ii) we ignore the movement of the pipe itself, and postulate a sinusoidal driving force $F = F_o \sin\left(\frac{2\pi t}{T}\right)$ where F_o is the maximum force, **T** the wave period, and **t** the time elapsed.

(iii) the bearing resistance force is the sum of two components, one proportional to displacement **e** and given by **Kbre**π (from equation (27)), the other, **Ww**, the product of velocity de/dt and a non-linear damping coefficient ϕ.

If the mass of the buoy is M_B then the equation of motion will be

$$M_B \frac{d^2e}{dt^2} = F_o \sin\left(\frac{2\pi t}{T}\right) - \phi \frac{de}{dt} - Kbr\pi e \qquad (47)$$

dividing by M_B and rearranging gives

$$\frac{d^2e}{dt^2} + \phi' \frac{de}{dt} + K'e - F_o \sin\left(\frac{2\pi t}{T}\right) = 0 \qquad (48)$$

where:

$$\phi' = \frac{\phi}{M_B}$$

$$K' = \frac{Kbr\pi}{M_B}$$

$$F_o' = \frac{F_o}{M_B}$$

Equation (48) describes the forced oscillation of a system subject to non-linear damping (ie ϕ' is not constant, but a function of displacement **e**); as such, a solution for **e** as a function of time **t** can not be found simply as in the common case. A resort to some numerical method, such as the Runge-Kutta-Nyström method (ref 12), seems necessary,but before this can be done we have to allocate values to all the coefficients used in the calculation; this process begins in the next section, in which the permanent magnet repulsion system is analysed to find the optimum arrangement.

4. THE PERMANENT-MAGNET REPULSION SYSTEM

4.1 Specification

The purpose of the magnet system was briefly outlined in sections 2.2 - 2.4, but a more detailed summary of the requirements it must meet is as follows:

(i) to completely support the maximum predicted static load of 5.1 tonnes f on the buoy and 6.5 tonnes f on the counter-weight (see section 1.2).

(ii) to maintain the narrow fluid film thickness **h** at a small value (say $\leqslant$ 20mm) at all times, closing almost to zero as the maximum cyclic load is approached. There are two reasons for this, namely to ensure the development of high film pressures, and also to reduce the amount of relative radial movement of the magnet sheet and the yaw-prevention mechanism to which it is coupled.

(iii) to achieve (i) and (ii) allowing for possible circumferential misalignments of opposing magnets (notwithstanding the yaw-prevention mechanism).

(iv) for at least 20 years in a marine environment, without loss of performance.

(v) to be economic, i.e. use as little magnetic material as possible, consistent with the above requirements.

4.2 Magnetic Material

The most suitable material for our purpose is anisotropic strontium ferrite, one of the newer members of the ferrite class. These in general combine high values of *intrinsic coercivity* **Hci** with "square-loop" *intrinsic hysteresis* curves: the value of **Hci** represents the minimum strength of reversed (demagnetising) field required to completely demagnetise the material, while a square-loop intrinsic

hysteresis curve is characteristic of a material which suffers practically no demagnetisation when exposed to reversed fields of strength less than the critical value **Hci**. These properties are particularly important in repulsion applications, where opposing magnets exert mutually demagnetising fields. The other property of interest is the intrinsic flux density or magnetisation **J**, a measure of the magnetic strength per unit volume of material, and hence of the force it can exert on other magnetised bodies. For strontium ferrite, typical values (at 25°C) are **Hci** = 3.18×10^5 amp metres^{-1}, and **J** = 0.34 tesla. These are by no means the highest values available: magnets of the rare-earth cobalt type such as $PrCo_5$ can have **Hci** = 7.24×10^5 Am^{-1} and **J** = 0.72T (ref 13); because repulsion force is proportional to $\mathbf{J}^2$, such magnets may exert four to five times the force of the equivalent ferrites.

However, the rare-earth cobalts are still very expensive, and are also subject to oxidation, whereas the raw material for ferrites is cheap and plentiful, and the final product practically inert (ref 14) due to the high oxidation state of its constituent elements. Furthermore, experiments have shown that ferrites actually have somewhat better "square-loop" characteristics than the more powerful rare-earth cobalts (ref 13), thus rendering them more truly "permanent" magnets. When two newly-magnetised ferrite magnets are forced together in repulsion, an irreversible loss of magnetisation **J** of perhaps 2 - 3% occurs; after this **J** remains pretty well constant no matter how often the magnets are brought into contact.

Changes in temperature may cause reversible and/or irreversible demagnetisation of ferrites, for which **J** decreases by 0.19% and **Hci** increases by 0.2 - 0.5% (based on their room-temperature values) for every degree rise in temperature over a range -100°C to +400°C (ref 14). The result of this could be to increase the initial 'knock-down' demagnetisation mentioned above, for magnets operating at sea-temperatures (say 6-13°C). Because the variation in sea-temperature is so small, however, subsequent changes in **J** can be disregarded.

4.3 Calculation of Magnetic Forces

When the intrinsic flux density J of a permanent magnet material can be assumed constant and uniform, calculations of attractive or repulsive forces between two or more magnets may be achieved relatively easily. As we saw above, this applies to the ferrite magnets proposed for the power-buoy bearing. Mathematically, the magnets may be treated in one of the following three ways:

(i) as three-dimensional distributions of elementary magnetic dipoles.

(ii) by replacement of the pole-face with surfaces of uniform "magnetic charge" distribution.

(iii) by replacement of the magnet with an equivalent air-cored solenoid.

Each method should be judged only by its ease of use, as the results obtained by all three will be identical. The first method (dipole distribution) has been employed by Yonnet for passive magnetic bearings (refs 15 & 16), while the second (surface charge distribution) has been used by Baran (refs 17 & 18) and by Coffey at al (ref 19) in studies of vehicle levitation by permanent magnets. This was the application examined too by Borcherts (ref 20), but using the third (solenoid) technique, also used by Tsui et al (ref 13) in their comparison of different permanent magnet materials.

For the power-buoy bearing, solenoid mathematics were used; the initial analysis was that of a rectangular permanent magnetic block of finite length levitated above another of infinite length - the "magnetic track" approximation. Note, however, that the resulting forces per unit length (ie of the upper magnet) would be the same had we considered both magnets to be infinitely long. The situation is illustrated in Fig 11. The two magnets are replaced by equivalent current-carrying windings as shown, with the current density being given by J/μ_o amps metre , where μ_o is the magnetic constant with value $4\pi \times 10^{-7}$ Hm^{-1}. From the expression for the forces mutually exerted by incremental elements of two conducting loops (ref 21) we may

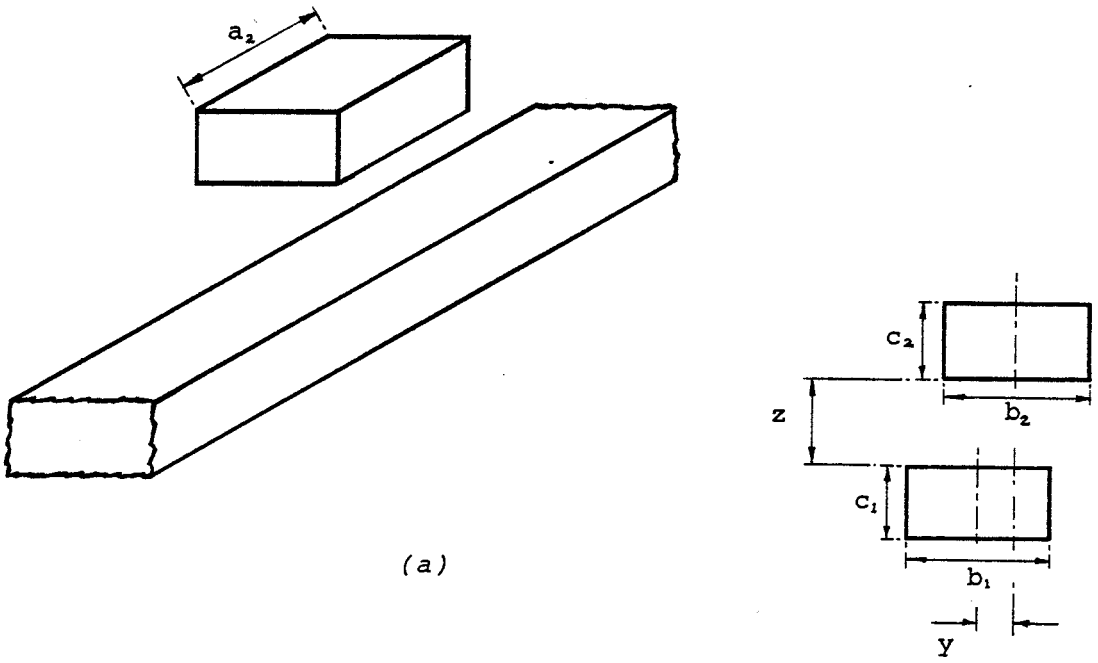

(a)

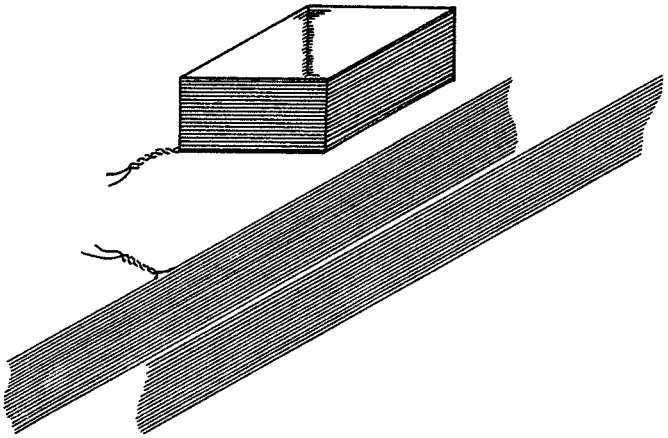

(b)

Fig 11 *(a) Permanent magnet of finite length a_2 in repulsion with a magnet of infinite length; cross-sectional dimensions as shown.*

(b) Mathematically equivalent solenoid windings.

integrate the total force of interaction of our two rectangular solenoids. As the process is somewhat lengthy, only the final results are quoted here. Using the dimensional notation of fig 11, the vertical force **Fz** is given by

$$F_z = \frac{J_1 J_2 a_2}{4\pi\mu_0} \sum_{i=1}^{2} \sum_{j=1}^{2} \sum_{k=1}^{4} n_{ij} b_{ij} \rho_k \left\{ 2 \tan^{-1}(z_k) + z_k \ln\left[b_{ij}^2 (1 + z_k^2) \right] \right\} \tag{49}$$

and the horizontal force by

$$F_y = \frac{J_1 J_2 a_2}{4\pi\mu_0} \sum_{i=1}^{2} \sum_{j=1}^{2} \sum_{k=1}^{4} n_{ij} b_{ij} \rho_k \left\{ 2 z_k \tan^{-1}(z_k) - \ln\left[b_{ij}^2 (1 + z_k^2) \right] \right\} \tag{50}$$

where the following notation is used:

k	ρ_k	z_k
1	1	$\frac{z}{b_{ij}}$
2	-1	$\frac{z + c_1}{b_{ij}}$
3	-1	$\frac{z + c_2}{b_{ij}}$
4	1	$\frac{z + c_1 + c_2}{b_{ij}}$

i	j	n_{ij}	b_{ij}
1	1	1	$y + \frac{1}{2}(b_2 - b_1)$
1	2	-1	$y - \frac{1}{2}(b_2 + b_1)$
2	1	-1	$y + \frac{1}{2}(b_2 + b_1)$
2	2	1	$y - \frac{1}{2}(b_2 - b_1)$

For multiple magnet systems as envisaged in the bearing, the total force on any magnet is simply the vector sum of all the individual forces. In calculations of bearing clearances and stiffness etc., we disregard the forces which magnets on the same side of the bearing exert on each other; these must be taken into account, however, when considering the method of securing the magnets in place.

4.4 Optimising the Magnet System

To minimise the cost of this major component, we must find the least volume of magnetic material which will provide the desired force. The first point to note is that *heteropolar*, or alternating, magnetic track layouts are more efficient than *homopolar* ones (see fig 12); this can be explained with reference to fig 12(b) which shows part of a homopolar system.

Because of the angles involved, the forces exerted on the upper magnet by non-central lower magnets are actually attractive and tend to decrease the total repulsion; by alternating the polarity of the rows, however, we may reverse this effect for increased efficiency, BUT note that the horizontal forces ($\mathbf{F_2(y)}$ in fig 12(b)) then change from restoring (positive spring) forces to destabilising (negative spring) forces. Note also that the directly opposing magnets have zero horizontal force ($\mathbf{F_2(y)} = 0$) but that any deviation from alignment gives rise to an increasing offset force; passive magnetic repulsion (or attraction) can only ever exist in unstable equilibrium, as a result of Earnshaw's theorem (ref 22).

From fig 11 and equation (49) the levitation force per unit volume $\mathbf{F_V(z)}$ for a single track interaction is given by

$$F_V(z) = \frac{F_z}{a_2(b_1c_1 + b_2c_2)} \qquad (51)$$

and from the expression for **Fz** (49) it is seen that $\mathbf{F_V(z)}$ is independent of length $\mathbf{a_2}$; we have essentially a two-dimensional problem in which we have to minimise the value of $\mathbf{F_V(z)}$ with respect to the geometric variables $\mathbf{b_1}$, $\mathbf{c_1}$, $\mathbf{b_2}$, $\mathbf{c_2}$, **y** and **z**. The multiple-track system optimisation is also two-dimensional, but with an extra variable corresponding to the lateral pitch of the tracks (see figs 12(a) and (c)).

Much work has been done by Baran (18) and Henning (23) on the optimisation of multi-track systems for high-speed vehicle levitation: iterative computer programs were developed with the aim of minimising the amount of magnet used in the track, for a given vehicle weight

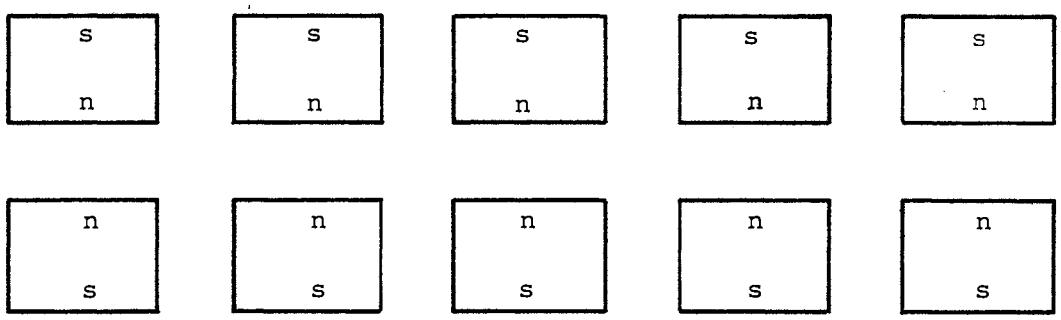

(a)

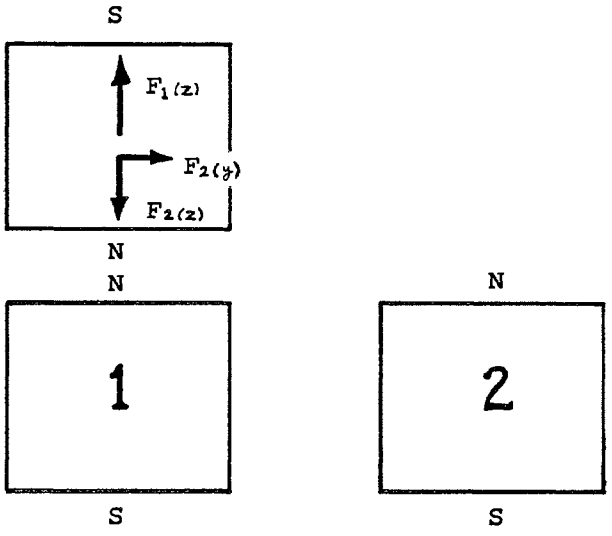

(b)

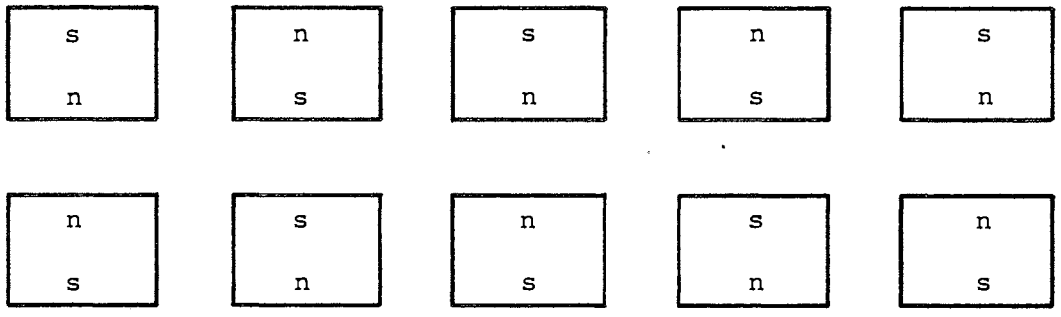

(c)

Fig 12 (a) Homopolar magnet arrangement, showing (b) the neighbouring-row effect which decreases total repulsion; the effect is turned to advantage by the use of a heteropolar system (c).

and clearance **z**. In such "magnetic-railway" applications, the volume of the track magnets vastly outweighs that in the vehicle - this will not be the case in the power-buoy bearing, where the "track" length on the mooring pipe may be less than twice the "vehicle" length, i.e. the length of the bearing elements for both buoy and counterweight.

A program of the type described (23) might easily be adapted to our requirements; alternatively, a new programme could be specifically written, although this would obviously take rather longer. In the meantime an approximate solution is proposed on the following basis:

- because the "track" and "vehicle" lengths are not greatly different in length, and because we are not concerned with the levitated weight of either side of the bearing, we will not differentiate between them when we come to optimise the cross sectional area for a given force and clearance.

- we will restrict ourselves to optimisation of a single-track system as described above, and subsequently investigate the effect of varying the lateral pitch for optimised geometries.

The computer optimisation for vertical repulsion force **Fz** for geometries such as shown in fig 11, is accomplished as follows. A constant area **A** is specified such that $\mathbf{A} = \mathbf{b}_1\mathbf{c}_1 + \mathbf{b}_2\mathbf{c}_2$ and it is assumed that $\mathbf{b}_1 = \mathbf{b}_2$ and $\mathbf{c}_1 = \mathbf{c}_2$ at all times: the justification for this is detailed later. Because $\mathbf{c}_1 = \mathbf{A}/2\mathbf{b}_1$ and hence is not an independent variable, then

$$\frac{dF_z}{db_1} = \left(\frac{\partial F_z}{\partial b_1}\right)_{c_1} + \left(\frac{\partial F_z}{\partial c_1}\right)_{b_1} \times \frac{dc_1}{db_1} \qquad (52)$$

where the partial derivatives $\frac{\partial F_z}{\partial b_1}$ and $\frac{\partial F_z}{\partial c_1}$ may be found analytically from equation (49).

Now $\frac{dc_1}{db_1} = -\frac{c_1}{b_1}$, and hence

$$\frac{dF_z}{db_1} = \left(\frac{\partial F_z}{\partial b_1}\right)_{c_1} - \frac{c_1}{b_1}\left(\frac{\partial F_z}{\partial c_1}\right)_{b_1} \qquad (53)$$

Because of our assumptions, the only independent variable is b_1, and furthermore a maximum of the function "force per unit area" is also a maximum for force itself, as area **A** is constant. Our problem is reduced to that of finding the maximum of **Fz** with respect to b_1; this is done by iteratively seeking the root of the function $\frac{dF_z}{db_1}$ which corresponds to a local maximum, and recording the corresponding values of b_1, c_1 and **Fz**. This process is repeated at increasing values of clearance **z** keeping offset **y** constant, until the following curves may be plotted:

(a) maximum available vertical force per unit length vs clearance **z** for a given offset **y** and cross sectional area **A**.

(b) optimum values of b_1/c_1 corresponding to the force in (a), vs clearance **z**, with **y** and **A** constant.

alternatively, curves of optimum force vs offset at constant clearance may be drawn, but these are not generally as useful.

The curves corresponding to (a) and (b) for zero offset (**y** = 0) are shown in fig 13. Note that instead of plotting maximum force per unit length directly against clearance, we have plotted "force per unit length $/J^2/$ **z**" vs $z/\sqrt{A}$. In this way the force figures are made independent both of scale and magnetisation, and the clearance is made dimensionless. The purpose of this is illustrated by the following practical example.

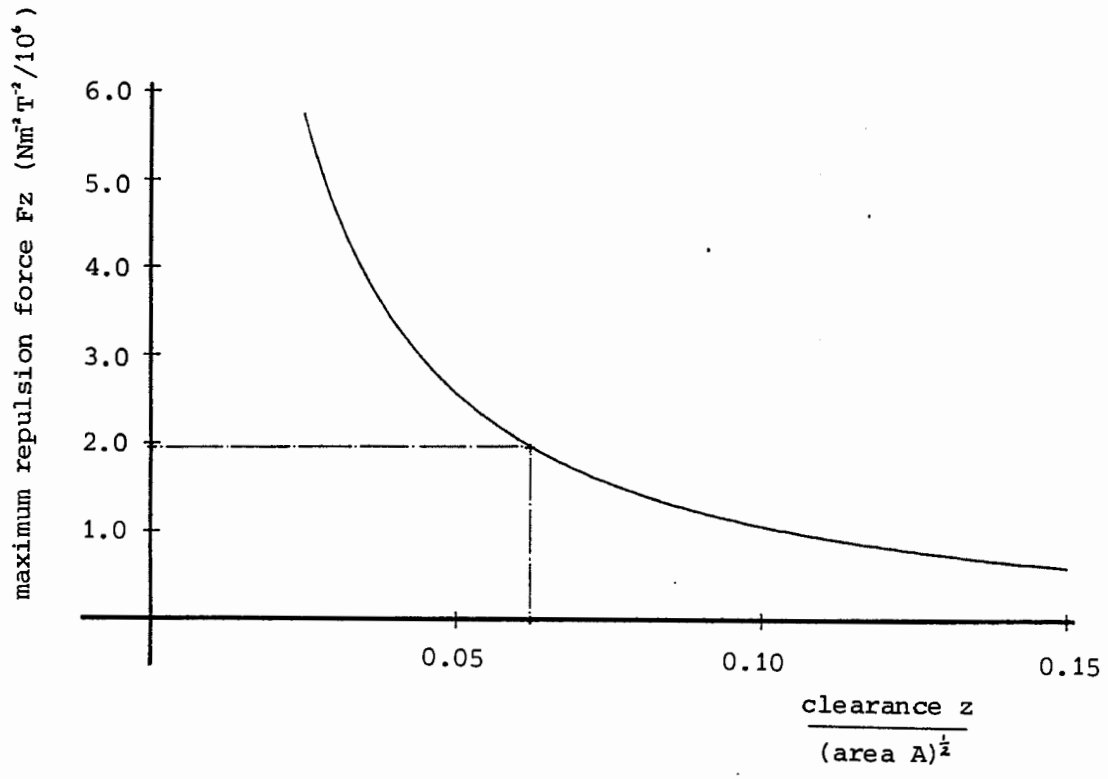

(a)

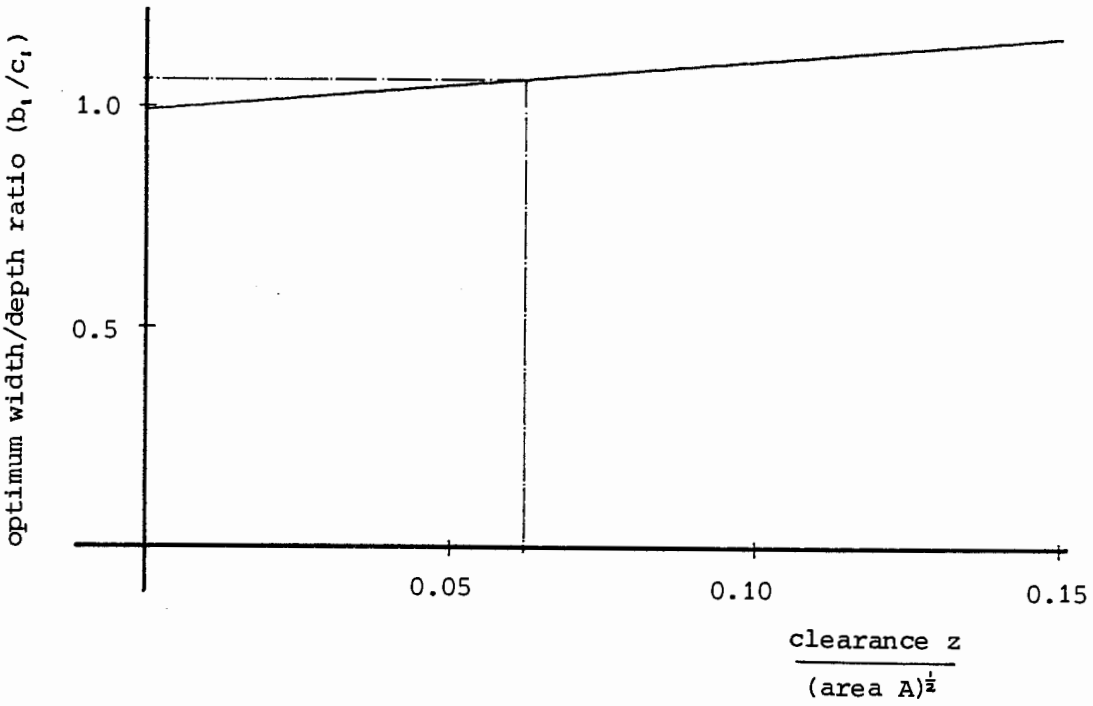

(b)

Fig 13 (a) Maximum-possible vertical repulsion force for a single track interaction (units are scale-independent).
(b) Optimum ratio of magnet dimensions corresponding with (a).

Supposing we want a force of $1000 Nm^{-1}$ for a single-track system, at a clearance of 5mm, using ferrite magnets with J = 0.32 tesla. We first convert our force requirement into the scale-independent units of fig 13(a), the value being: $1000/0.32^2/0.005 = 1.95 \times 10^6 Nm^{-2}T^{-2}$. From the curve 13(a) the corresponding value of clearance $\mathbf{z}/\sqrt{\text{area } \mathbf{A}}$ is ca 0.062, hence $\mathbf{A} = (5mm/0.062)^2$ i.e. $2\mathbf{b}_1\mathbf{c}_1 = 6500mm^2$. From the curve 13(b) the optimum value $\mathbf{b}_1/\mathbf{c}_1$ at this point is 1.06; solving the two equations given by

$$2 b_1 c_1 = 6500\ mm^2$$

$$b_1/c_1 = 1.06 \qquad (54)$$

we get the required dimensions $\mathbf{b}_1$ = 58.7mm, $\mathbf{c}_1$ = 55.4mm; the total volume of 1m length of such a track would be $6.5 \times 10\ m^{-3}$.

A similar computer-optimisation program to that described above was written in which all the magnet dimensions $\mathbf{b}_1$, $\mathbf{b}_2$, $\mathbf{c}_1$ and $\mathbf{c}_2$ were treated as independent variables (i.e. with no area constraint applied, and no assumptions about similar magnet cross-sections); for a given clearance **z** and offset **y** the calculation returned the maximum possible force per unit volume **Fv** and optimum dimensions whereby the partial derivatives $\frac{\partial F_v}{\partial b_1}$, $\frac{\partial F_v}{\partial b_2}$, $\frac{\partial F_v}{\partial c_1}$ and $\frac{\partial F_v}{\partial c_2}$ were all zero-valued. It was found that no matter what values of **y** and **z** were used, the resulting optimum dimensions always had $\mathbf{b}_1 = \mathbf{b}_2$ and $\mathbf{c}_1 = \mathbf{c}_2$. It is for this reason then, that we assume similar magnet dimensions in our constrained optimisation procedure.

We now attempt to optimise the real case of the power-buoy bearing magnets, and begin with the following (provisional) specifications:

(i) ferrite magnets to be used, with density $\rho = 4600 kgm^{-3}$ and magnetisation J = 0.32 tesla.

(ii) the total length of mooring pipe laid with magnetic tracks to be 50m.

(iii) two annular bearing elements (as in fig 5) to be used, one each for the buoy and counterweight, both 10m in length.

(iv) the total maximum static loads to be distributed evenly along the bearing surfaces, corresponding to 5.0kN per metre for the buoy element and 6.4kN per metre for the counterweight (see section 1.2).

(v) with zero load, the magnetic pole separation to be approximately 5mm.

(vi) the magnetic spring characteristics should not change significantly as a result of lateral (yaw) misalignment; let us say that a "maximum allowable" lateral offset **y** of 5mm should reduce the magnet pressure by no more than 10% in the equilibrium static load situation, and a "disastrous" misalignment of 10mm should reduce it by no more than 30%.

(vii) with reference to fig 7, the bearing inner radius **r** to be 0.70 - 0.75m, and the circumferential length of the surface between splines (based on a 4-spline bearing) to be ca 1000mm.

(viii) two cases to be considered, in which the total amount of magnetic material will not exceed firstly 15 tonnes and secondly 20 tonnes.

The optimal solution will inevitably be a compromise between the two extremes of a few rows of very large magnets, and many rows of very small ones. Magnet size is critical for several reasons. The advantages, firstly, of using large magnets are:

(a) lower cost per unit weight; most magnets are cut from blocks of standard dimensions and the fewer cutting operations required, the lower the cost: we have been quoted ca £1,200 per tonne for relatively large blocks (150mm x 100mm x 25mm) and around £3500 per tonne for smaller ones (100mm x 30mm x 20mm).

(b) the greater the magnets' size in relation to a possible offset **y**, the less will be the corresponding decrease in repulsion. Large magnets, then, will be more able to meet requirement (vi) above.

(c) the fewer magnets there are, the easier (and cheaper) will be the construction.

On the other hand, however, the advantages of using small magnets are:

(d) higher force to weight ratios: repulsion forces vary as the square of the linear dimensions of a magnet system, while weight varies as the cube, hence force per unit weight is inversely proportional to scale (this argument holds only when comparing systems in which all the relative proportions are the same, including clearances and offsets (refs 14 and 24))

(e) better use of the heterpolar effect: for the same amount of material, the provision of many rows of small magnets would mean a closer-pitched arrangement than a few rows of large ones, and hence an increase in the neighbouring-row repulsion described earlier (see p 43 and fig 12)

(f) better compliance characteristics for the magnet-sheet.

4.5 Comparison of Possible Magnet Systems

Let us consider the area of the mooring pipe between two splines (see fig 5), covered by magnetic tracks; from 4.4 (ii) and (vii) this equals 50m x 1m, i.e. $50m^2$. Adding to this the equivalent areas on the upper and lower moving elements gives $70m^2$, representing one-quarter of the total magnetic bearing area. If 15 tonnes of magnet are to be used, then the amount distributed over this area will be 3.75 tonnes, or 0.0536 tonnes per metre *total* length (i.e. adding all three components together). The corresponding figures for the 20-tonne case are, respectively, 5.0 tonnes and 0.0714 tonnes per metre; henceforth the figures in brackets refer to the 20-tonne case. Assuming a magnet density of $4600kgm^{-3}$ this corresponds to $11.65 \times 10^{-3} m^3$ ($15.53 \times 10^{-3} m^3$) of magnetic material per metre length, or a cross sectional area, between two splines, of $11.65 \times 10^3 mm^2$ ($15.53 \times 10^3 mm^2$) we shall compare systems of 10, 15, 20, 25, and 30 parallel rows between splines.

Dividing the total area by the number of rows gives the cross sectional area of a single magnetic track, e.g. for 10 rows the figure would be $1165mm^2$ ($1553mm^2$); the total area **A** of two opposing magnets is twice this figure, ie $2329mm^2$ ($3106mm^2$). We continue by expressing the desired clearance **z** of 5mm as a dimensionless function of **A** by dividing by $\sqrt{\mathbf{A}}$; i.e. $5/\sqrt{2329} = 0.104$ (0.090).

From fig 13(a) the maximum available force per metre/(clearance x J^2) is found to be $1.003 \times 10^6 Nm^{-2} T^{-2}$ ($1.218 \times 10^6 Nm^{-2} T^{-2}$); taking **J** = 0.32T and converting to force per metre gives 514 Nm^{-1} (624 Nm^{-1}). Figure 13(b) gives the corresponding optimum ratio of magnet width to depth, in this case 1.108 (1.093), from which the dimensions themselves may be found: the area of a single magnet is $1165mm^2$ ($1553mm^2$) and hence the depth $\mathbf{c} = \sqrt{1165/1.108}$ i.e. 32.4mm (37.7mm), and the width $\mathbf{b} = \sqrt{1165 \times 1.108}$, i.e. 35.9mm (41.2mm).

The pressure exerted by a single magnet pair one metre long and *neglecting* heteropolar interactions is found by dividing the force per unit length by the magnets' circumferential pitch, which is in

turn equal to the distance between splines (1m) divided by **n**, the number of rows. For **n** = 10 the pitch is 0.1m, and hence the pressure 5.14kPa (6.24kPa).

We now calculate the pressure available from a heteropolar system based on these dimensions, i.e. this time taking account of the neighbouring-row interaction described in section 4.4, and examine three cases:

(i) with zero lateral offset **y**
(ii) with **y** = 5mm
(iii) with **y** = 10mm

Summation of the forces is carried out by microcomputer program, and for the case being considered the resulting true pressure is 5.59 kPa (7.03 kPa) for **y** = 0, 5.11 kPa (6.55 kPa) for **y** = 5mm, and 4.12 kPa (5.54 kPa) for **y** = 10mm. The offset pressures represent respectively 91% (93%) and 74% (79%) of the fully-aligned pressure. This calculation process has been applied to each of the cases for n = 10, 15, 20, 25 and 30 rows between splines for both cases (15 and 20 tonnes total magnet material) and the results can be seen in tables 3 (15 tonnes) and 4 (20 tonnes). Note the effects of increasing the number of rows of magnets while decreasing their size: available pressure increases considerably, but at the expense of greater pressure losses for non-zero lateral offsets. Based on our earlier requirement to retain 90% pressure at 5mm offset, and 70% at 10mm offset we reject all but the 10 and 15-row systems in the 15 tonne case; using 20 tonnes, the 10, 15 and 20-row systems all meet the requirements.

The pressure exerted by each of the remaining systems is calculated over the range of clearances 0-20mm for comparison, and the results may be seen in figure 14. Of these remaining magnet arrangements, the optimum will be that which supplies the necessary pressure characteristics over the specified range of loads, but in doing so allows the least possible variation in pole separation **z**. The reasons

Number of rows n between splines	10	15	20	25	30
Circumferential pitch p (mm)	100	66.7	50.0	40.0	33.3
Cross sectional area bc of one magnet (mm^2)	1165	777	583	466	388
" " " A of magnet pair "	2330	1553	1165	932	777
Dimensionless clearance $z/A^{\frac{1}{2}}$	0.104	0.127	0.146	0.164	0.179
Maximum force per unit length (Nm^{-1})	513.5	388.7	317.8	267.3	233.8
Optimum magnet width/depth ratio b/c	1.108	1.134	1.155	1.176	1.192
" magnet width b (mm)	35.9	29.7	25.9	23.4	21.5
" " depth c "	32.4	26.2	22.5	19.9	18.0
Pressure neglecting heteropolar interaction (kPa)	5.14	5.83	6.36	6.68	7.02
Pressure including heteropolar interaction, offset y = 0mm (kPa)	5.59	6.86	8.01	9.07	9.96
" " " " " " 5 "	5.11	6.19	7.16	8.03	8.65
" " " " " " 10 "	4.12	4.83	5.46	5.90	5.75
Percent full pressure at offset y = 5mm (%)	91	90	89	89	87
" " " " " " 10 "	74	70	68	65	58
Percent pressure gained by heteropolar interaction (%, zero offset)	9	18	26	36	42

Table 3 Data for a 15-tonne magnet system. The magnet separation z is nominally 5mm (maximum static load case); cirumferential distance between splines = 1000mm, figures based on ferrite magnets with $\rho = 4600 kgm^{-3}$ and J = 0.32tesla.

Number of rows n between splines	10	15	20	25	30
Circumferential pitch p (mm)	100	66.7	50.0	40.0	33.3
Cross sectional area bc of one magnet (mm^2)	1553	1035	777	621	518
" " " A of magnet pair "	3106	2071	1553	1242	1035
Dimensionless clearance $z/A^{\frac{1}{2}}$	0.090	0.110	0.127	0.142	0.155
Maximum force per unit length (Nm^{-1})	623.7	475.4	388.7	331.0	290.9
Optimum magnet width/depth ratio b/c	1.093	1.115	1.134	1.151	1.166
" magnet width b (mm)	41.2	34.0	29.7	26.6	24.6
" " depth c "	37.7	30.5	26.2	23.1	21.1
Pressure neglecting heteropolar interaction (kPa)	6.24	7.13	7.77	8.28	8.74
Pressure including heteropolar interaction, offset y = 0mm (kPa)	7.03	8.85	10.48	11.73	12.94
" " " " " " 5 "	6.55	8.16	9.59	10.58	11.36
" " " " " " 10 "	5.54	6.76	7.76	8.07	7.44
Percent full pressure at offset y = 5mm (%)	93	92	92	90	88
" " " " " " 10 "	79	76	74	69	57
Percent pressure gained by heteropolar interaction (%, zero offset)	13	24	35	42	48

Table 4 As for table 3, but based on 20 tonnes of magnet material.

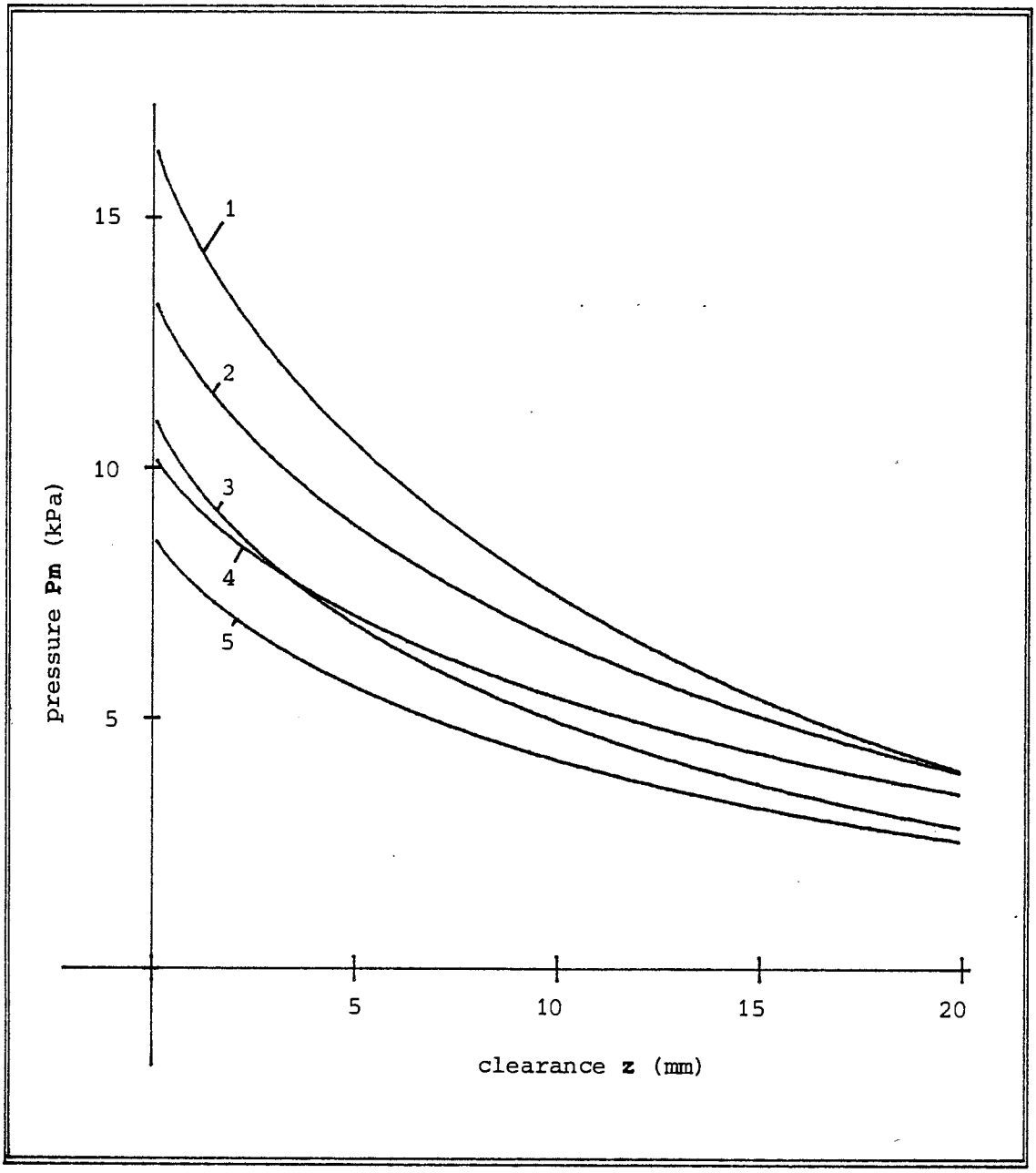

Fig 14 *Pressure vs clearance curves for five possible magnet arrangements, based on (1) 20 tonnes total material, 20 rows between splines, (2) 20 tonnes, 15 rows, (3) 15 tonnes, 15 rows, (4) 20 tonnes, 10 rows, and (5) 15 tonnes, 10 rows.*

for this were outlined in section 4.1 (ii), but to recap: a small range of clearance values **z** means a similarly small range for film thickness **h** (see fig 8), thus ensuring the build-up of high fluid pressures **Pw** as the buoy displacement **e** increases. We want the value of **h** to decrease to zero as the displacement reaches its maximum allowable value e_c. Also, a small clearance range means that there is little relative radial movement of the magnet-sheet and the yaw-prevention mechanism to which it is attached (described later, in section 5). However, a compromise is necessary - to fully support the static load **Ws**, the magnets must be allowed a sufficient range of movement **z** for their stiffness to provide the required force increase on one side of the bearing, and decrease on the other. We shall now examine this further in terms of the five remaining magnet arrangements.

For a maximum static load per unit axial length of **Ws/b** Nm^{-1} from equation (26) the approximate value for buoy radial displacement is given by

$$e_s = \frac{W_s}{K b r \pi} \quad metres \qquad (55)$$

where **r** is the bearing inner radius (metres) and **K** the mechanical spring rate of the compression cells (pressure increase per unit deflection, in pascals per metre). Now, the *maximum* inward radial displacement of the buoy is e_c observed at $\theta = 0$ to the load line-of-action, which occurs during cyclic loading. The corresponding maximum outward displacement is $-e_c$ at $\theta = 180°$, and hence the full excursion range is $2e_c$. We said that the fluid film thickness should tend to zero as **e** approaches e_c. There may seem to be an initial attraction for a system which allows **h** to decrease to such an extent that the surfaces should touch while there is still some distance to go before the cells fully discharge: a squeeze-film would then establish which would prevent actual contact, despite the displacement **e** having exceeded that value at which this should happen. However, the argument contains

a dangerous flaw: the effect could only work on the loaded side of the bearing when displacement was positive, ie inwards. As soon as the load was reversed the film pressure would disappear, leaving the two bearing surfaces pressed hard together by the action of the springs.

Let us specify that the film thickness **h** should never exceed say 20mm; this figure is subject to revision according to the results of hydrostatic pressure calculations and experiments. We further specify that the thickness of the plastic coverings on the bearing surfaces be 0.5mm; from fig 8 the minimum value of **z**, ie z_c is then 1mm. We set the maximum value of **z** at 20mm, and hence $h_{max.}$ at 19mm.

Because the magnet and spring pressures are always in equilibrium (refer to section 3.2, eqns (10) and (12)), the drop in magnet pressure **Pm** as **z** increases from 1 to 20mm must be matched by an equivalent drop in spring pressure **Ps** as the buoy goes through its full displacement excursion, i.e.:

$$P_m\ (z = 2mm) \;-\; P_m\ (z = 20mm) \;=\; K \Delta l \qquad (56)$$

neglecting the small contribution which Δz makes to the change in spring-length Δl we have

$$\Delta P_m\ (z = 2 \rightarrow 20mm) \;=\; 2 K e_c \qquad (57)$$

if we re-arrange this expression and combine it with equation (55) we may eliminate **K**, to give the following approximate expression which relates the maximum static displacement e_s and cyclic (i.e. maximum overall) displacement e_c

$$\frac{e_s}{e_c} \;=\; \frac{2 W_s}{\Delta P_m b r \pi} \qquad (58)$$

The maximum static load **Ws** was that predicted for the lower bearing element, namely 64kN, the length **b** = 10m, inner bearing radius **r** (including the magnet layer on the pipe surface) = 0.75m (say) and hence

$$\frac{e_s}{e_c} = \frac{2 \times 64 \times 10^3}{\Delta P_m \times 10 \times 0.75 \times \pi} \qquad (59)$$

$$\Rightarrow \quad \frac{e_s}{e_c} \simeq \frac{5400}{\Delta P_m} \qquad (60)$$

where **ΔPm** is in pascals, and is measured over the appropriate clearance range (in this case **z** = 1 - 20mm). The ratio e_s/e_c is important, being approximately equal to the proportion of water which has been expelled from the compressible cells (at **θ** = 0) under maximum static load conditions compared to their equilibrium volume; the lower the value of e_s/e_c the better, as it means a greater reservoir of water remains, ready to sustain any cyclic load. Although in practice the worst static loads predicted here are highly unlikely to occur in the absence of fairly heavy cyclic loads (ie due to wave action), we will discard any bearing system which is in danger of losing more than a given proportion of its water content under the maximum static load **Ws**, assuming this to occur in isolation from any wave action.

Let us say that the cells must retain at least 20% of their volume for **Ws** max, i.e. $e_s/e_c \leqslant 0.8$. For the five magnet systems left we find the values of pressure **Pm** at clearances of **z** = 1mm and 20mm from fig 14, and hence **ΔPm** over the same range. The corresponding values of e_s/e_c come directly from equation (60); a comparison of the five cases may be seen in table 5. Only three of these systems survive our constraint above, i.e. $e_s/e_c \leqslant 0.8$, namely those based on 20 tonnes with 15 and 20 rows of magnets, and that with 15 tonnes and 15 rows.

Total system tonnage (whole bearing)/tonnes	*20*	*20*	*20*	*15*	*15*
No of magnet rows between splines	*10*	*15*	*20*	*10*	*15*
Pressure Pm, clearance z = 1mm/kPa	*9.2*	*12.0*	*14.6*	*7.6*	*9.7*
" " " " 20mm "	*3.5*	*3.9*	*3.9*	*2.5*	*2.8*
Pressure difference ΔPm/kPa	*5.7*	*8.1*	*10.7*	*5.1*	*6.9*
Hence ratio e_s/e_c *(see equation (60))*	*0.95*	*0.67*	*0.50*	*1.06*	*0.78*

Table 5 Comparison of five magnetic repulsion arrangements, examining the maximum static load displacement e_s *in relation to the maximum allowable (cyclic-load) displacement* e_c.

4.6 Provisional System Dimensions

We now calculate the dimensions of the three systems which remained as a result of the optimisation procedure. Referring to fig 8, let us say that the equilibrium value of the radial distance **H**, given the symbol H_o, is to be 150mm. The dimension **d** is the radial depth of the magnet-retaining sheet; we will say that **d** will equal 1.25 times the magnets' depth. The value of $H_o - d - z$ gives the spring length ℓ at any position round the bearing, according to equation (16) in section 3.2; the minimum value of ℓ will be the spring's *solid height* (fully compressed). From equation (17), substituting e_c for the maximum buoy displacement $e\cos\theta$ (i.e. $\theta = 0$), and ℓ_s for the spring's solid height (including some safety margin) we have

$$\ell_s = H_o - e_c - d - z_c \qquad (61)$$

We said earlier that z_c = 1mm, and if we allow 15mm for ℓ_s then the maximum allowable deflection e_c is found from

$$e_c = 0.134 - d \quad metres \qquad (62)$$

an approximation for e_s the maximum static-load deflection is found from equation (60) once e_c is known. Although the spring rate **K** can be found from the approximate expression $K = Ws/br\pi e_s$ (from expression (26), section 3.2), we are able to find a more accurate estimate, and also the springs' equilibrium (i.e. uncompressed) length ℓ_e from equation (17) in section 3.2. Because spring pressure **Ps** equals magnet pressure **Pm**, for maximum positive displacement $e = e_c$, when z = 1mm, we have

$$P_s(z = 1mm) = K(\ell_e + e_c + d + 0.001 - H_o) \quad pascals \qquad (63)$$

and for maximum negative displacement $e = -e_c$ and z = 20mm:

$$P_s(z = 20mm) = K(\ell_e - e_c + d + 0.020 - H_o) \quad pascals \qquad (64)$$

From which we solve simultaneously for **K** and ℓ_e, where:

$$K = \frac{P_s\,(z = 1mm) - P_s\,(z = 20mm)}{2\,e_c + 0{\cdot}019} \quad Pa\,m^{-2} \qquad (65)$$

and

$$\ell_e = \frac{P_s\,(z = 1mm)}{K} + H_o - e_c - d - 0{\cdot}001 \quad metres \qquad (66)$$

The value of the magnetic pole separation z_o for zero load is more difficult to find: because we cannot express clearance **z** as an explicit function of pressure **Pm(z)**, we must use an iterative method. For this equilibrium condition **e** = 0, and hence from equation (18)

$$P_m\,(z_o) - z_o = \ell_e - (H_o - d) \qquad (67)$$

which is solved by trial-and-error using the data shown in fig 14; the value of ℓ_e - **(H_o-d)** is known in each case, and it is simply a matter of finding the combination of **Pm(z)** and **z** which satisfies equation (67) in each case.

4.7 Lateral Magnetic Forces

At this stage we consider another very important characteristic of each possible magnet system, namely the rise in lateral (instability) force with increasing offset **y**, caused by possible yaw misalignment. The lateral force calculation for a multiple magnet arrangement is carried out in exactly the same way as in the vertical force (i.e. pressure) case, except for the use of the appropriate expressions for **Fy** rather than **Fz** (see section 4.3 on magnetic forces). For each of the three systems still under consideration the lateral force per metre length for a single bearing panel (i.e. the magnet sheet between

two splines) was calculated with offset **y** increasing over the range 0 - 30mm. The clearance **z** was fixed at its minimum value of 1mm, at which the offset forces take on their highest values. The results for the three cases can be seen in fig 15. Note that the initial rise in lateral force also represents the steepest part of each curve, and also that the relationship is roughly linear in this region, i.e. with offset **y** in the approximate range of 0 - 3mm; the slope of the line here represents the maximum negative spring rate of the magnet system in the lateral direction, an important parameter in the design of the yaw-prevention mechanism.

Table 6 summarises the characteristics of the last three magnet systems, according to the calculations described above. Points of interest include the values of $e_c - e_s$ representing the difference between the maximum possible and maximum static-load-only displacements. For the 15-tonne system, $e_c - e_s$ is ca 22mm, while the value for the 20-tonne, 20-row system is over twice this figure. Note also that the equilibrium (ie zero-load) values of magnet separation z_o and hence of equilibrium fluid film thickness h_o are all roughly similar, with the former all around 5mm.

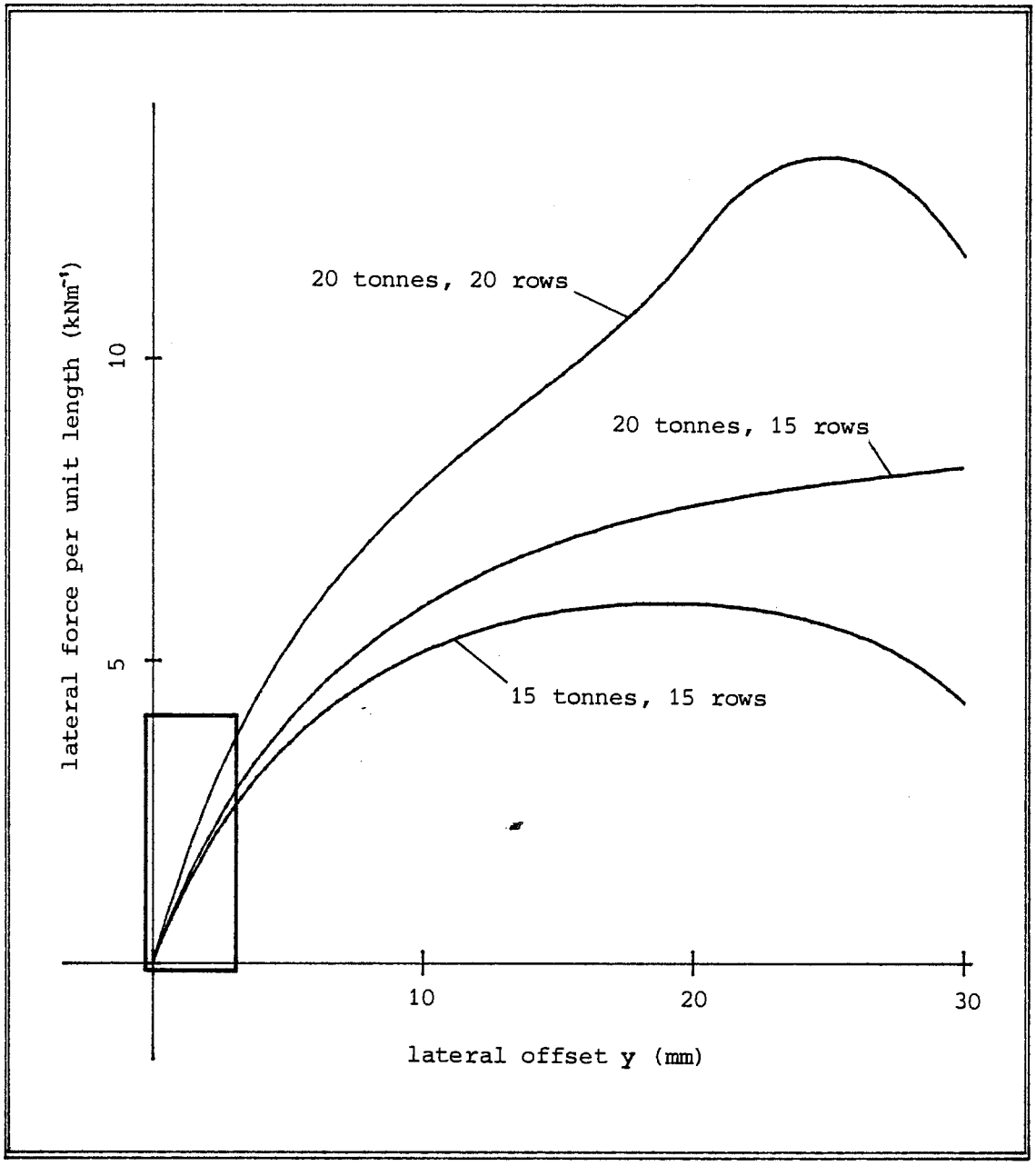

Fig 15 *Lateral (instability) force for three magnet systems as a function of the lateral offset y, constant clearance z = 1mm. Maximum negative spring rate is roughly linear over the range y = 0-3mm (see table 6 for calculated values).*

Total magnet system weight/tonnes	*20*	*20*	*15*
No. of magnet rows per panel (between splines)	*20*	*15*	*15*
Magnet circumferential pitch/mm	*50*	*66.7*	*66.7*
" *width* b/*mm*	*29.7*	*34.0*	*29.7*
" *depth* c/*mm*	*26.2*	*30.5*	*26.2*
" *sheet thickness* d/*mm*	*33*	*38*	*33*
Maximum-possible relative displacement e_c */mm*	*101*	*96*	*101*
Approx. maximum static-load displacement e_s */mm*	*51*	*64*	*79*
$e_c - e_s$ */mm*	*50*	*32*	*22*
Maximum magnet pressure Pm *(z = 1mm)/kPa*	*14.6*	*12.0*	*9.7*
Magnet pressure decrease ΔPm, *z = 1-20mm/kPa*	*10.7*	*8.1*	*6.9*
Mechanical spring pressure rate K/*kPam*$^{-1}$	*48.3*	*38.4*	*31.2*
Free (unloaded) length l_e *of equivalent compression springs/mm*	*317*	*328*	*326*
Equilibrium (zero-load) magnet pressure Pm/*kPa*	*10.0*	*8.6*	*6.7*
" " " " *pole separation* z_o */mm*	*5.7*	*5.5*	*5.3*
" " " *film thickness* h_o */mm*	*4.7*	*4.5*	*4.3*
Pre-compressed length l_o *of equivalent springs (where* $l_o = H_o - d - z_o$*)/mm*	*112*	*106*	*112*
Maximum negative spring rate for a single panel (lateral force per unit length, per mm offset y*)/Nm*$^{-1}$*mm*$^{-1}$	*1250*	*920*	*870*

Table 6 *Data for the three optimal magnetic repulsion systems, of all those originally considered. The equilibrium radial clearance* H_o *is nominally 150mm.*

5. DESIGN DETAILS

5.1 The Cell System

In fig 16 a cross-section of a possible bearing configuration is shown. The main differences between this design and the schematic design shown in fig 4 are in the spring system. Helical coil compression springs have been used in the compression cells, but the force required to precompress them is not now supplied by the bearing outer surface, but by a second spring system: this second system consists of tension springs which circumferentially link the free ends of the compression cells all the way round the bearing. This arrangement is proposed in order to minimise the tangential forces experienced by either the cells or the magnet sheet. The cells must be allowed to collapse radially (ie along their axes) only, with no tendency to buckle or shear.

To facilitate this, the tension springs must combine a low spring rate with the ability to supply a large enough force to precompress the cells; we essentially require a "constant force" tension spring. The precompression force is easily calculated: if a tension member of radius **r** is required to precompress the cells by a given pressure **Ps**, then the tension spring force per unit axial length of the bearing is simply the product **Ps x r**. In the design shown, the circumferential pitch of the cell's free ends changes by about 10% during the compression cycle (from zero load to maximum deflection), and the tension springs must supply **Psr** newtons per metre axial length constantly over this range of deflections. It should be noted that a constant standing force exerts no tangential load on the cells, but that any *changes* in the spring tension will, and this load must necessarily be accommodated by the cells without shearing. This tangential force will also be experienced by the yaw-prevention mechanism (described below), and for these reasons it must be kept to an absolute minimum; this would be achieved in practice by using large numbers of low-rate springs along the length of the bearing.

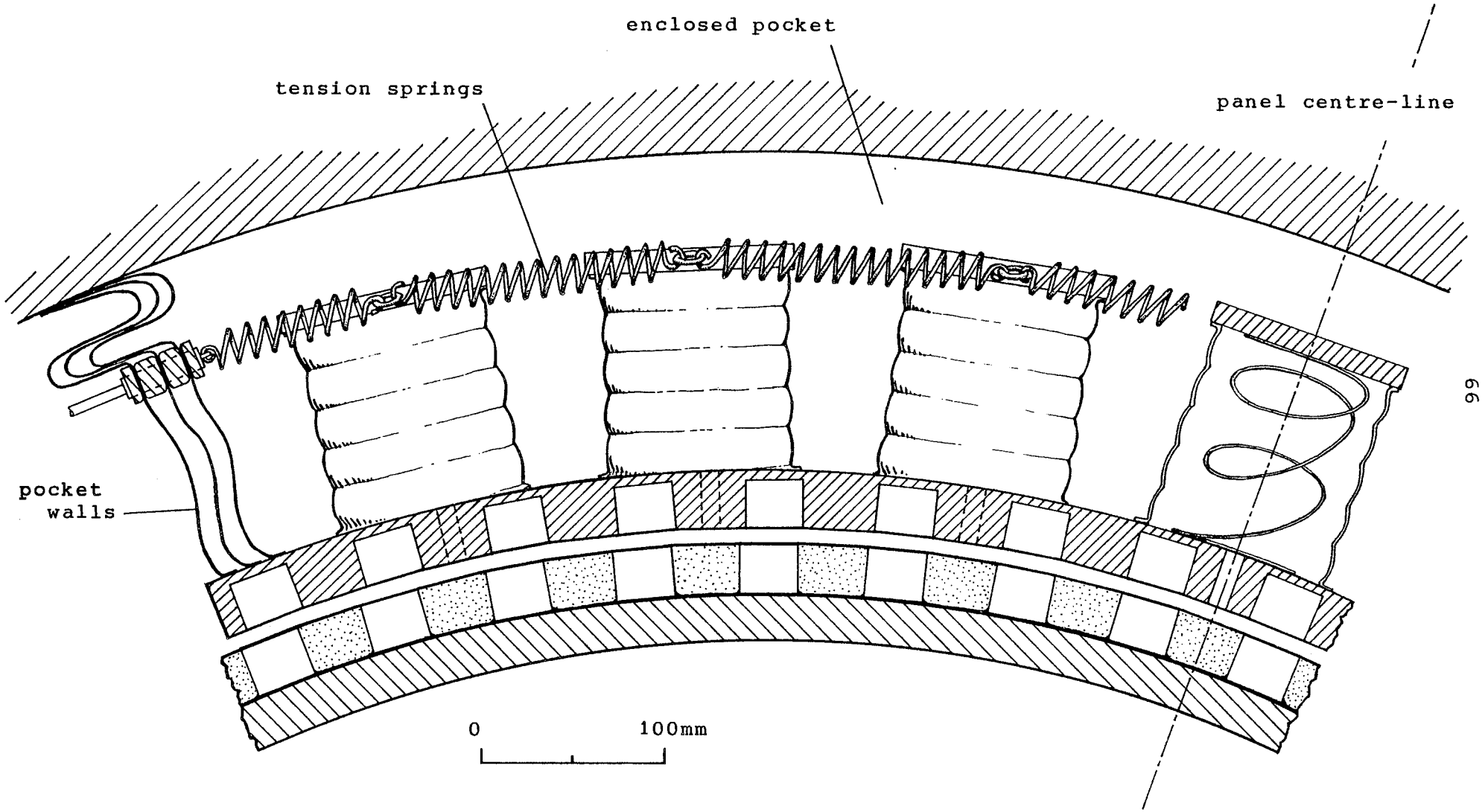

Fig 16 Cross-section of proposed bearing (unloaded).

Note also from fig 16 that the force to compress the cells is transmitted via a trapped pocket of water, enclosed at its base by the magnet sheet, and at its edges by flexible walls. It is this arrangement which allows us to decouple the tangential shear movement of the buoy from the cell layer. When a load is applied to the buoy, the water in the pocket cannot escape, so the pocket volume decreases by compressing the cells; on the other side of the bearing the cells expand correspondingly. On the compressed side of the bearing, such an arrangement may be subject to cavitation at the point of load reversal; this will largely depend on the squeeze-film characteristics during the second half of the cycle, and may only be a problem in the upper regions of the bearing (where ambient pressure is lowest). This design may also require some form of yaw restraint other than the flexible fabric walls: experimental yaw-force measurements will indicate whether this is the case.

5.2 Yaw Prevention Mechanism

This is illustrated in figures 17 and 18. Roller-carriages are spring-coupled between adjacent magnet sheets, and run axially along the splines which are welded to the surface of the mooring pipe.

Although it may seem unsatisfactory to introduce rolling wheels into a bearing which was designed to replace such components, it should be stressed that the forces on the yaw-prevention rollers will be very small compared with the main bearing loads. The splines are formed from lengths of folded steel strip, the folding process acting to establish their straightness. The reason for using angled splines of the kind illustrated is to ensure that any wear of the rolling wheels, assuming it to occur equally on both sides of the spline, does not introduce lateral misalignment problems: the carriage should simply ride lower on the spline. The carriage is attached to the magnet sheets on each side by torsion springs which are designed to allow the sheet to move through a small vertical range parallel to its central axis (see fig 16). The arrangement shown envisages the springs being in 'tension' with the roller carriage being pulled down onto the spline

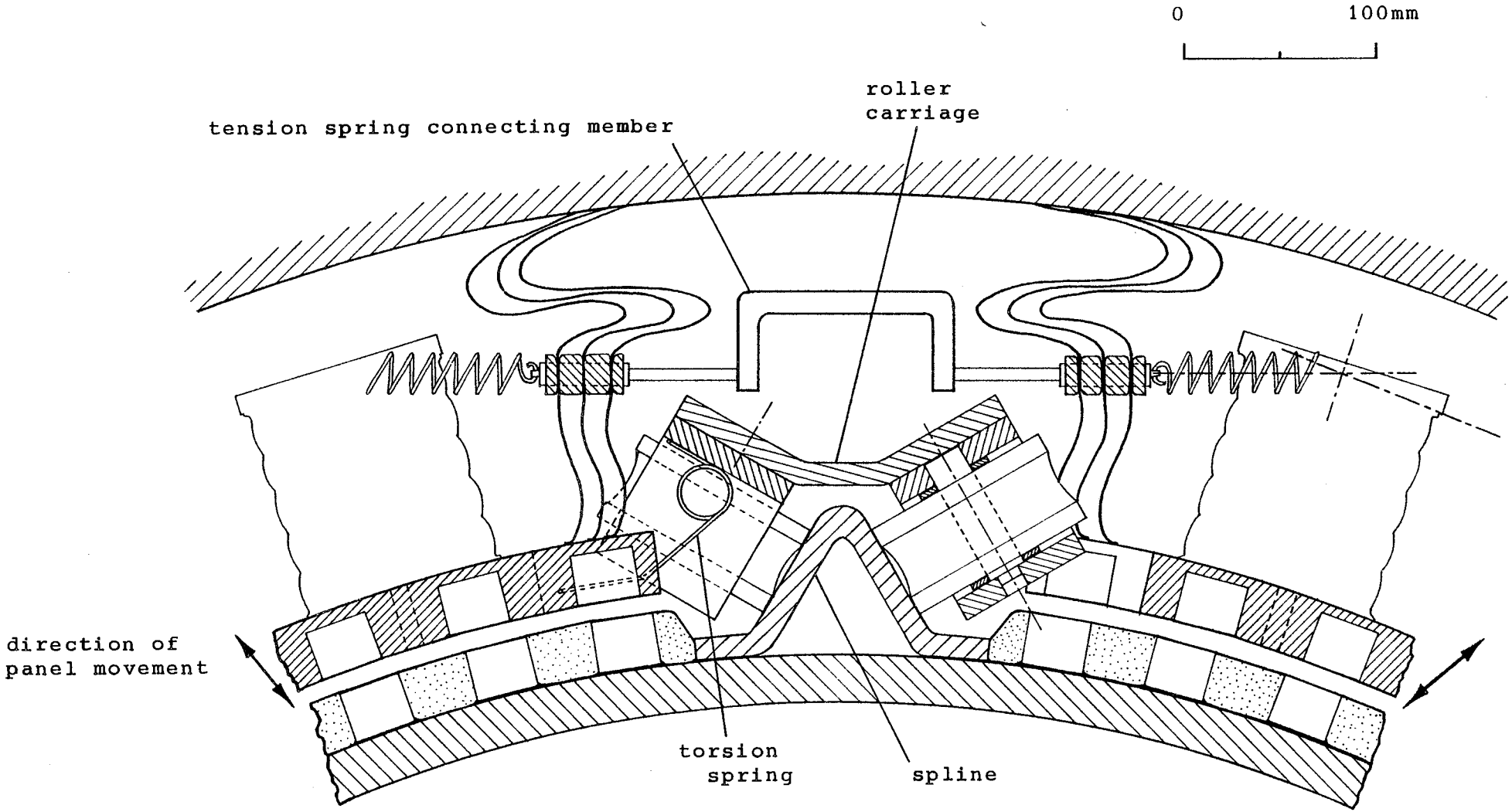

Fig 17 Yaw prevention mechanism.

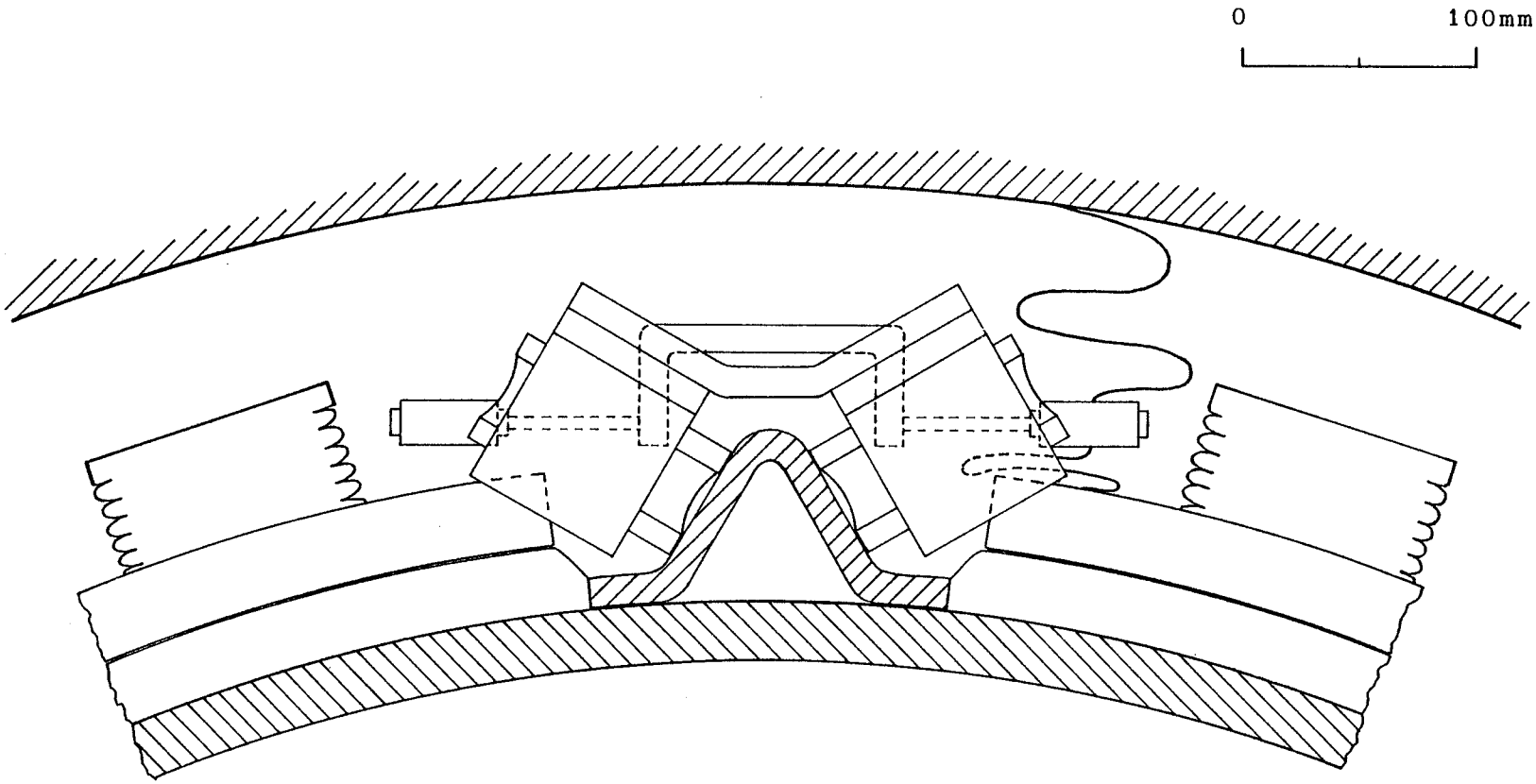

Fig 18 Yaw prevention mechanism, with the bearing nearing full compression.

by the magnet sheet, with a force which depends on the springs' stiffness in the vertical direction; this will be low by design. The reaction at the spline will therefore not be constant in the system shown, but will increase as the magnets' clearance tends to zero; yaw resistance will then be at its greatest just when it needs to be, ie when the magnetic force and lateral instability are at a maximum.

A U-shaped channel connects the tension-spring member of one bearing panel with the next, via rigid connecting members in the flexible cell walls; these need not be completely leak-proof, but will have a high impedance to water flow. The connecting channel allows the tension springs to operate throughout the full range of bearing radial excursions, as shown in fig 18, in which the bearing is nearing its fully collapsed state. The roller carriages are accommodated in periodic gaps in the cell/spring system, so that the U-channel is not impeded.

One or more of the splines may be of somewhat different design, to allow the use of a disk-brake latching system: for this purpose the roller carriages and tension spring connecting channels would require to be suitably modified. It would also be necessary to encroach further into the buoy itself in order to allow room for the larger spline. The latching brake would be most easily situated above the bearing element in the buoy assembly, and could be connected to the buoy by a lever arm, capable of moving radially to allow for the relative movement of the buoy and mooring pipe; the brake itself could be mounted on a roller-guided carriage which travelled along the spline rails in the same manner as the yaw prevention mechanism.

5.3 The Complete Assembly

Figure 19 is an impression of the complete structure. The upper and lower bearing elements as shown are rigidly connected together

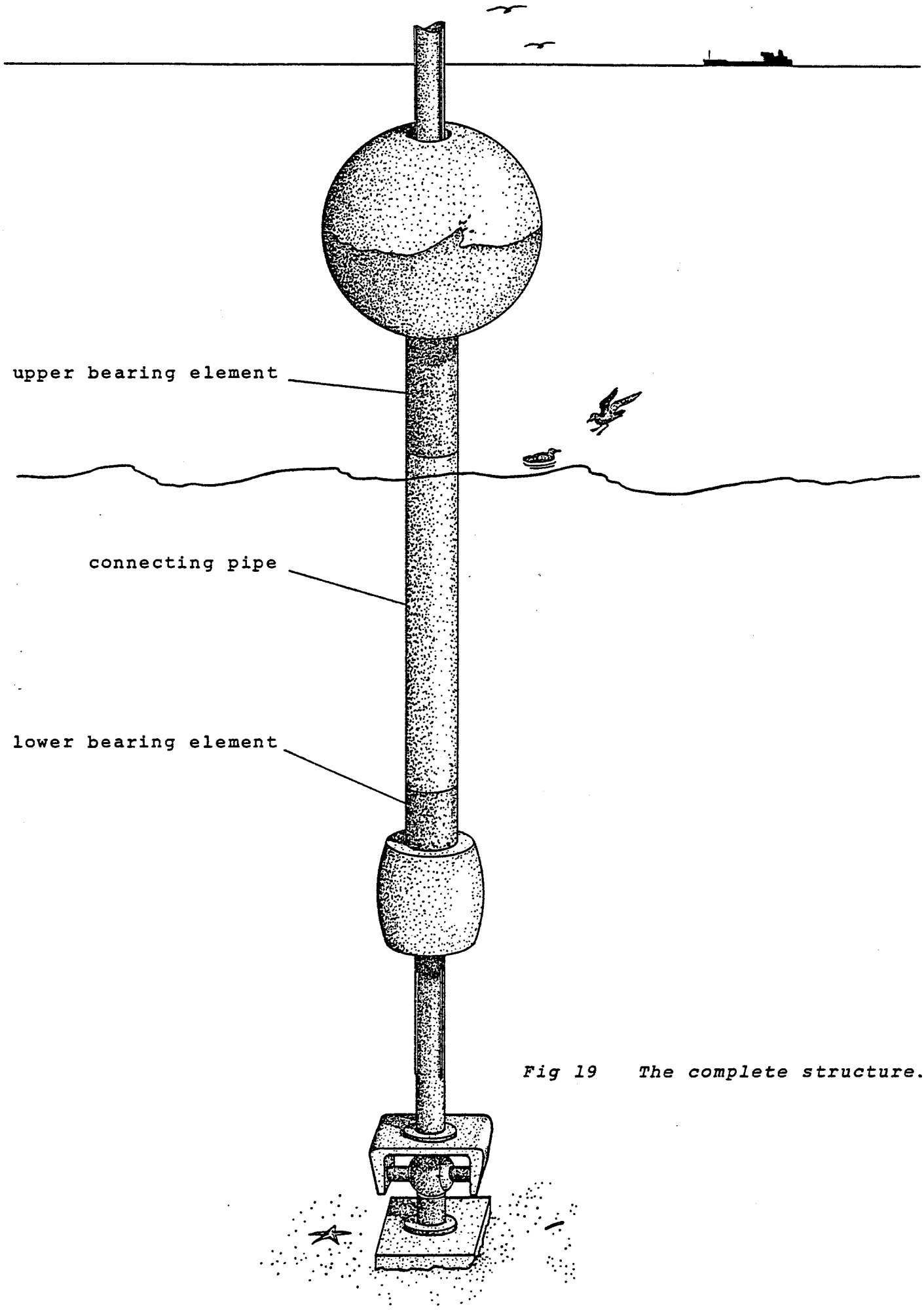

Fig 19 The complete structure.

by a steel pipe of approximate diameter 2m; this serves the following purposes:

(i) it allows us to set the upper element fairly low down in the power buoy, so that it remains below the splash zone at all times. Although the simple laws of leverage predict that the bearing surge resistance will require to be somewhat higher - by about 15 to 20% - than if it were centrally positioned in the buoy, this increase is not a problem; the advantage of such an arrangement is, however, very great indeed, as it ensures that the cell system is always 'wet' with no danger of the water draining away when the buoy is latched in the upper position. Furthermore, if the lower bearing element is situated high relative to the counterweight, the total length of the magnetic tracks on the mooring pipe surface may be reduced (by perhaps 10 - 15 metres).

(ii) we completely remove the danger of pitching of either the buoy or the counterweight, with the loads now being distributed evenly along the axial lengths of both elements.

(iii) we can maintain a partially trapped volume of water between the two bearing elements. This has two important consequences:

a) the squeeze-film effect will be enhanced: because the volume of water in the connecting pipe cannot change, each bearing element will now experience axial leakage of water at one end only (ie at the upper end of the buoy element, and the lower end of the counterweight element) where it is open to the sea.

b) the time taken for complete water exchange, although dependent on the prevailing level of wave action, will be long: this has great importance with respect to the marine fouling problem. One of the most effective methods of preventing fouling is continuous low-level chlorination; the concentration of toxin used is of little importance compared with the length of time for which it is administered (ref 25). Indeed, the

continuous presence of as little as 0.02 - 0.05 ppm of chlorine has been shown to be enough to deter the settlement and growth of hard fouling species resistant to much higher intermittent doses of the biocide. This concentration corresponds to only one or two grammes of biocide in the entire bearing system of the power buoy. Chlorine generation by on-board electrolysis of seawater is possible, and has been recommended as particularly suitable for wave-energy converters (ref 26) due to the ready availability of electricity, the absence of harmful ecological side-effects, and the safety of installation and operation.

The proposed system would require local structural strengthening where the connecting pipe was joined to the buoy and counterweight; one way of achieving this would be to make the pipe an integral part of both structures. As long as the dynamic behaviour of the power buoy was not greatly affected, the weight of the pipe (approximately 37 tonnes for a pipe 30m long, 2m diameter and wall thickness 25mm) could be offset by using a lighter counterweight. The increased drag due to the exposed part of the pipe, about 20m long, must be taken into account in calculation of bearing loads (see section 1.2).

The problem of corrosion of metal elements in the bearing must also be investigated; at present the likeliest choice of material for the springs is beryllium copper or beryllium bronze, which exhibit excellent corrosion fatigue endurance in sea water (refs 26, 27).

REFERENCES

1. *Standard Handbook of Lubrication Engineering*, McGraw-Hill Book Co., New York, 1968:
Rabinowicz, E., chapter 1, "Dry Friction".
Archibald, F. R., chapter 7, "Squeeze Films".

2. Hals, T., "Description of Motion and Loads of Wave Power Buoy Type N2", revised 14.01.82, private communication.

3. Budal, K., et al, "The Norwegian Wave-Power Buoy Project", *Second International Symposium on Wave Energy Utilisation*, Trondheim, June 1982.

4. Massey, B. S., *Mechanics of Fluids*, 4th edn., Van Nostrand Reinhold (U.K.) Ltd., Berkshire, 1979.

5. Jeffrey, D. C., et al, *Edinburgh Wave Power Project Second Year Report*, Edinburgh University, September, 1976.

6. Barwell, F. T., *Bearing Systems, Principles and Practice*, Oxford University Press, Oxford, 1979.

7. Castelli, V., et al, *Design Guide for Hydrostatic Axisymmetric Compliant -Surface Thrust Bearings*, Technical Report No.16, Lubrication Research Lab., Columbia University, New York, 1969.

8. McCutchen, C. W., "Mechanism of Animal Joints", *Nature*, vol.184, pp 1284-5, 1959.

9. McCutchen, C. W., "Physiological Lubrication", *Symposium on Lubrication and Wear in Living and Artificial Human Joints*, Paper No.1, Institute of Mechanical Engineers, London, April, 1967.

10. Kuzma, D. C., "Fluid Inertia Effects in Squeeze Films", *Applied Scientific Research*, vol.18, pp 15-20, 1967.

REFERENCES (contd.)

11. Estimated viscous drag losses in power buoy bearing, private communication to Professor Falnes, 2.12.82.

12. Kreyszig, E., *Advanced Engineering Mathematics*, 4th edn., John Wiley and Sons, New York, 1979.

13. Tsui, J. B., et al, "The Effect of Intrinsic Magnetic Properties on Permanent Magnet Repulsion", *IEEE Transactions on Magnetics*, vol.MAG-8, No.2, pp 188-94, June 1972.

14. McCaig, M., *Permanent Magnets*, Pentech Press, London, 1977.

15. Yonnet, J. P., "Passive Magnetic Bearings with Permanent Magnets", *IEEE Transactions on Magnetics*, vol.MAG-14, No.1, pp 803-5, September 1978.

16. Yonnet, J. P., "Permanent Magnet Bearings and Couplings", *IEEE Transactions on Magnetics*, vol.MAG-17, No.1, pp 1169-73, January 1981.

17. Baran, W., "Optimierung eines Permanentmagnetischen Abstützungssystems für Spurgebundene Schnellverkehrsmittel", *Z. Angew. Physik*, vol.32, pp 216-8, 1971.

18. Baran, W., "Der Augenblickliche Stand und die Weitere Entwicklung auf dem Gebiet der Permanentmagnetischen Abstützungssysteme für Spurgebundene Schnellverkehrsmittel", *Intern. J. Magnetism*, vol.3, pp 103-11, 1972.

19. Coffey, H. T., et al, "The Feasibility of Magnetically Levitating High Speed Ground Vehicles", *US Federal Railroad Administration Report No.FRA-RT-72-39*, Stanford Research Institute, California, February 1972.

20. Borcherts, R. H., "Mathematical Analysis of 'Permanent' Magnet Suspension Systems", *Journal of Applied Physics*, vol.42, No.4, pp 1528-9, March 1971.

REFERENCES (contd.)

21. Kip, A. F., *Fundamentals of Electricity and Magnetism*, McGraw-Hill Kogakusha, Tokyo, 1969.

22. Earnshaw, S., "On the Nature of the Molecular Forces which Regulate the Constitution of the Luminiferous Ether", *Transactions of the Cambridge Philosophical Society*, vol.7, Part 1, pp 97-112, 1839.

23. Henning, G., "Optimierung einer Gleichgepolten Magnetanordnung als Abstützungssystem für eine Magnetschwebebahn", *Technische Mitteilungen Krupp, Forschungsberichte*, vol.31, 1973.

24. McCaig, M., "Permanent Magnets for Repulsion Systems", *Electrical Review*, vol.169, pp 425-8, 1961.

25. Picken, M. J., and Fitzgerald, G. M. F., *Report on the Environmental Factors Relating to the Bristol Cylinder Wave Energy Device*, Scottish Marine Biological Association, Dunstaffnage, Oban, September 1981.

26. Hudson, J. A., et al, *Materials Aspects of Wave Energy Converters*, Final report, AERE Harwell, April 1981.

27. Wahl, A. M., *Mechanical Springs*, McGraw-Hill Book Co., New York, 1963.

ACKNOWLEDGEMENTS

I would like to express my thanks to my supervisor, Stephen Salter, for his help and advice in preparing this report, and also to Jo Nicholson, for patiently typing it.

The financial assistance of John Laing plc, London, is gratefully acknowledged.